Monte Carlo Study of Effects of Phantom Size, Radial Position, and Depth on Photon Beam Calibration

PIRS–507

A. Booth and D.W.O. Rogers
National Research Council of Canada
Ottawa, Canada K1A 0R6

Phone: (613) 993-2715
Fax: (613) 952-9865

E-mail: [redacted]
drogers@physics.carleton.ca

August 1995

Abstract

The EGS4 Monte Carlo simulation system and the user codes SPRRZ and BEAM_phantom have been used to estimate, for typical photon radiotherapy photon beams, the effects of phantom size, radial position and depth in phantom on the calculated Spencer-Attix water to air stopping-power ratio (SPR). This stopping-power ratio is the major determinant of the variation with beam quality in an ion chamber's absorbed dose to water calibration factor. Beam qualities ranging from ^{60}Co to 24 MV have been investigated. Results show that for a 100 cm^2 circular beam incident on the front surface from a point source at an SSD of 100 cm: the central axis stopping-power ratio varies by less than 0.1% for phantoms with areas between 100 cm^2 and 3600 cm^2; the stopping-power ratio varies with radial position only slightly more than this, with the largest effects near the edge of the smallest phantom; and for all beams the difference in stopping-power ratio between depths of 5 and 10 cm is less than 0.05% although the stopping-power ratio near the surface is up to 1.3% higher. The small size of the variation in stopping-power ratio as a function of radial position in the field and of phantom size implies that the stopping-power ratio also has a negligible variation for changes in field size around 100 cm^2, certainly less than 0.1% going from 100 cm^2 on the surface to 100 cm^2 at the depth of measurement. Finally the variation in the dose as a function of phantom size is shown to be up to 1.2% at a depth of 5 cm or 3.5% at 15 cm depth. These latter results suggest that field size specification may be phantom size dependent.

Contents

1 Introduction

When doing absorbed dose calibrations of ion chambers, or for purposes of dosimetry protocols, it is useful to know the expected variation in the calibration factor as parameters related to the phantom are varied. In standard notation[1], the calibration factor is given by:

$$\mathrm{N_{D,w}} = \frac{\mathrm{D_w}}{MP_{\mathrm{ion}}} = \frac{\left(\frac{W}{e}\right)_{\mathrm{air}}}{\mathrm{m_{gas}}} \left(\frac{\overline{L}}{\rho}\right)_{\mathrm{air}}^{\mathrm{water}} P_{\mathrm{wall}} P_{\mathrm{repl}} \qquad [\mathrm{Gy/C}] \tag{1}$$

The value of $\left(\frac{\overline{L}}{\rho}\right)_{\mathrm{air}}^{\mathrm{water}}$ varies by over 5% with photon beam quality whereas the other factors are either constant or much less dependent on beam quality (typically 1% variations or less, and much of the variation in P_{wall} is via variation in stopping-power ratios). Thus the variation in stopping-power ratio (SPR) likely dominates the variation in the calibration factor $\mathrm{N_{D,w}}$. This report primarily studies this variation in $\left(\frac{\overline{L}}{\rho}\right)_{\mathrm{air}}^{\mathrm{water}}$.

If stopping-power ratios vary dramatically with phantom size, then calibration procedures and dosimetry protocols would have to take this into account with care. Fortunately, for the 100 cm^2 beams studied in detail in this document, a variation of <0.1% is found in all cases and thus phantom size does not affect the calibration factor.

A second possibility is that the stopping-power ratio varies strongly as a function of radial position in the beam. In this case, issues concerning chamber size might become important. Again, this variation is shown to be negligible (<0.1%).

A related concern is that the stopping-power ratio might vary with the beam area on the surface (or depend on whether the beam size is specified at the surface or at the depth of measurement). We have not done calculations on this specific point because the lack of variation with phantom size and with radial position implies a similarly small variation with beam size (this is a form of the reciprocity theorem[2]).

Another issue concerns the depth of calibration. If the stopping-power ratio varies strongly with depth, then the depth of calibration and use must be controlled. Fortunately, again the variation in the central axis stopping-power ratio with depth is shown to be negligible, <0.05% variation between 5 and 10 cm depth. However, as reported previously (see ref[3] and references therein), there is a substantial increase in the stopping-power ratio close to the surface in the region of non-equilibrium, reaching a maximum of 1.3% in a 24 MV beam.

Finally, a related but conceptually different issue has been addressed. The dose (as opposed to stopping-power ratios discussed above) at each point in a phantom depends on the size of the phantom to a certain extent. This would play a role in clinical practice where reference dosimetry is done in a small phantom but applied in a large phantom (patient) or in a standards laboratory if different sized phantoms were used in the process of establishing an absorbed dose standard. To the extent the variations with phantom size are different at different depths, these calculations could show the extent to which beam quality specification depends on phantom size. Unfortunately, the calculations have not been optimized to study this aspect of the problem, but the current data indicates the issue is worth pursuing further.

The remainder of this report consists of a brief description of the calculations done followed by a graphical presentation of the data with little analysis past that given above. Nor have the results been compared to other values in the literature since no attempt at a thorough review has been made.

1.1 Method of Calculation

Calculations of stopping-power ratios are done with the NRCC user code SPRRZ which has been described briefly and used in several publications[3, 4, 5]. All calculations use the ICRU Report 37 stopping powers[6] as implemented in EGS4[7]. The value of Δ for the stopping-power ratios is 10 keV in all cases. This code has cylindrical symmetry and incident beams are from a point source, 100 cm away from the phantom surface in a vacuum. The incident circular beams have an area of 100 cm^2. The spectra of the incident beams are from Rogers *et al.* for the ^{60}Co beam[8] and from Mohan *et al.* for the accelerator spectra[9]. Calculations with these spectra and this code have been carefully benchmarked against other calculations (see ref [3, 4]).

The dose calculations in phantom have been done using the BEAM code[10] since, for central axis depth dose curves it has a range rejection algorithm which is more efficient than that in the standard user code DOSRZ.

1.2 Description of Phantoms

For the smallest phantom examined, the radius is 5.642 cm (100 cm^2) and its depth is 20 cm. The schematic in Figure 1 shows the phantom with the scoring regions for the simulation.

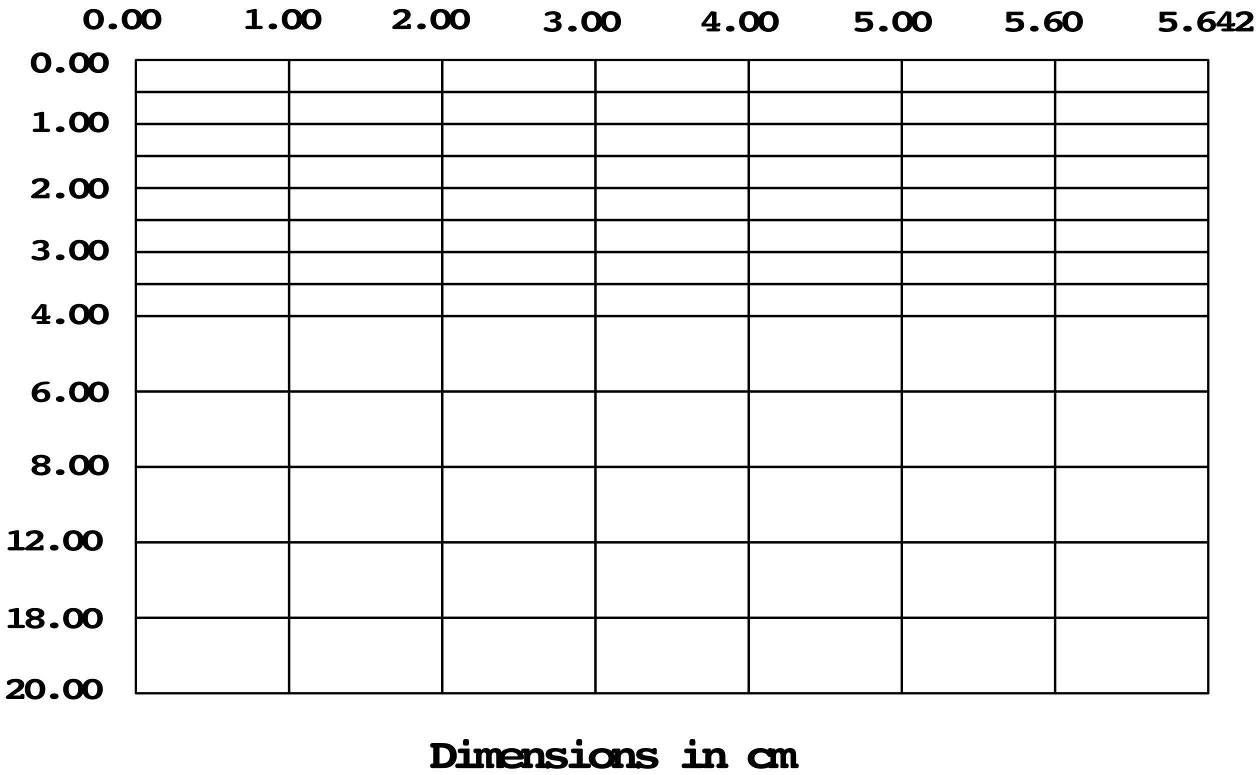

Figure 1: $10^2 cm^2$ phantom

For the 400 cm^2 phantom, the radius is 11.284 cm and the depth is 20 cm. It's dimensions are included in Figure 2.

For the 900 cm^2 phantom the radius is 16.926 cm and its depth is 30 cm. It's dimensions are included in Figure 2.

For the 3600 cm^2 phantom the radius is 33.851 cm and its depth is 60 cm. It's dimensions are included in Figure 2.

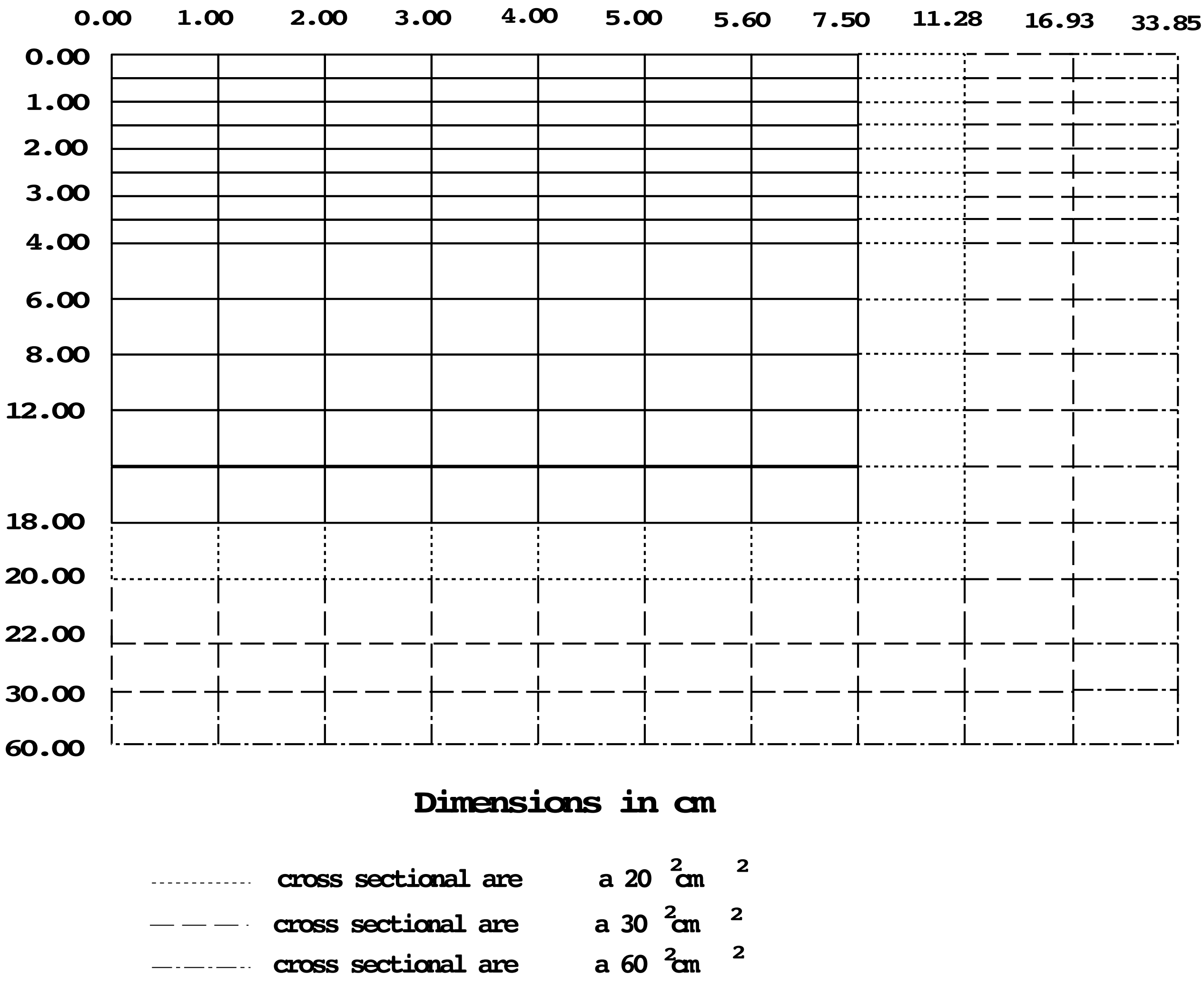

Figure 2: 20^2cm^2, 30^2cm^2, and 60^2cm^2 phantoms

2 SPR vs Phantom Radius

The following graphs show how the SPR varies with the overall size of the phantom at depths of 5 cm, 7 cm, 10 cm, and 15 cm for different radiation point sources 100 cm from the phantom front. The beam area is 100 cm^2 in all cases. The SPR data used for these graphs is from the inner most scoring region (1 cm radius) at each of the specified depths. Each SPR data point has a statistical uncertainty of no more than 0.02%, and often much better. The major conclusion is that there is no systematic effect at the 0.1% level.

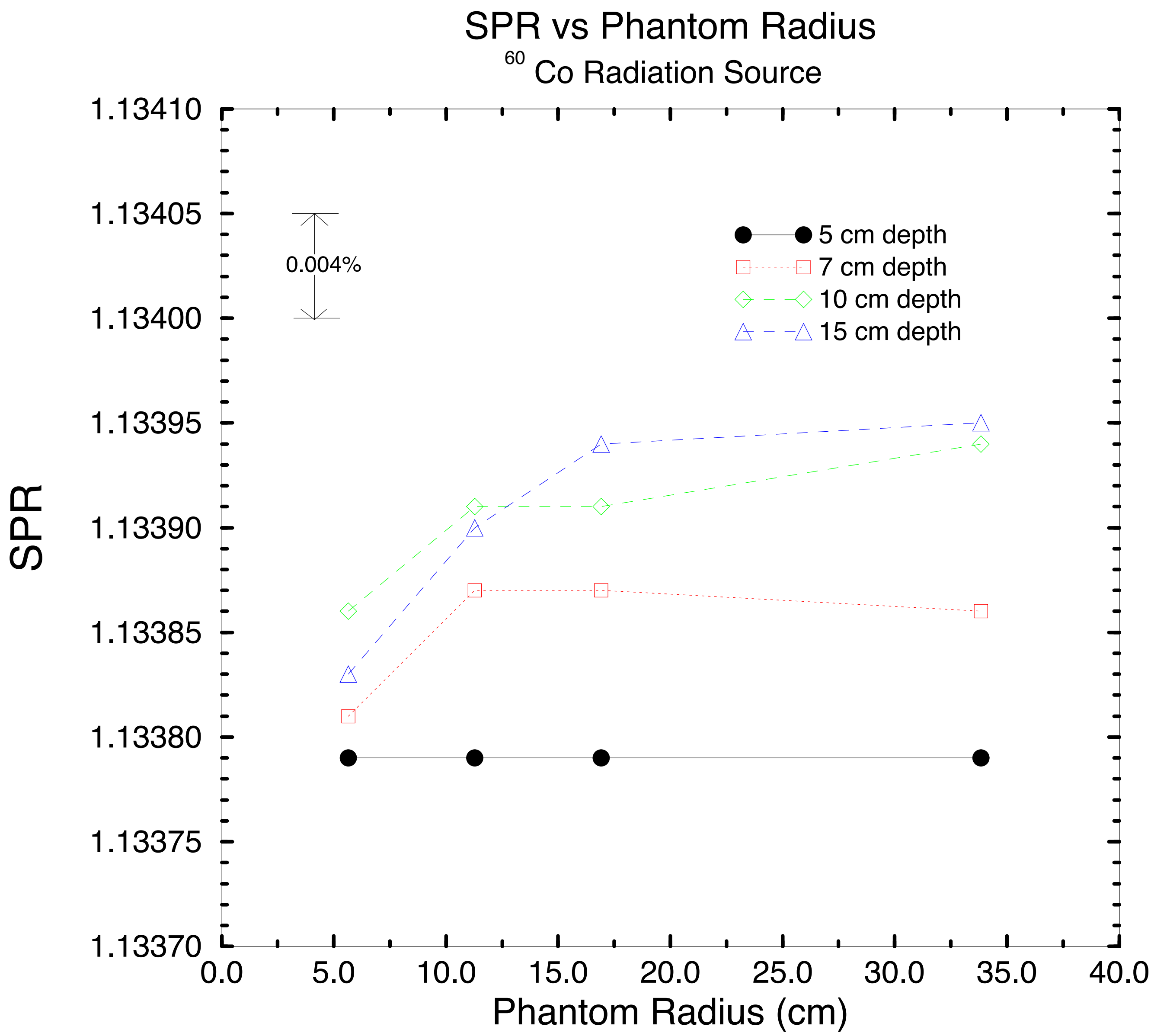

Figure 3: SPR vs phantom radius for ^{60}Co source

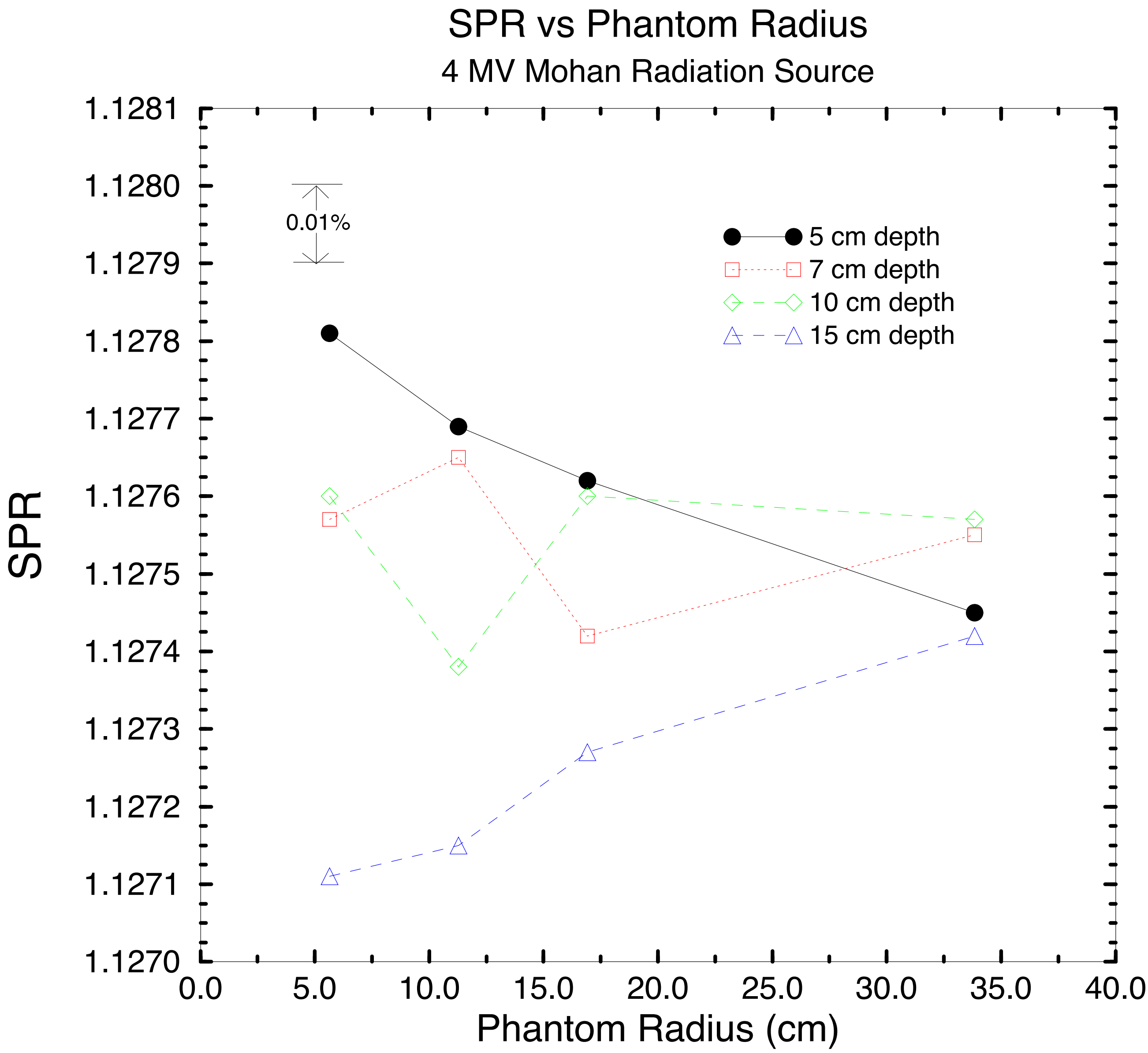

Figure 4: SPR vs phantom radius for 4 MV Mohan source

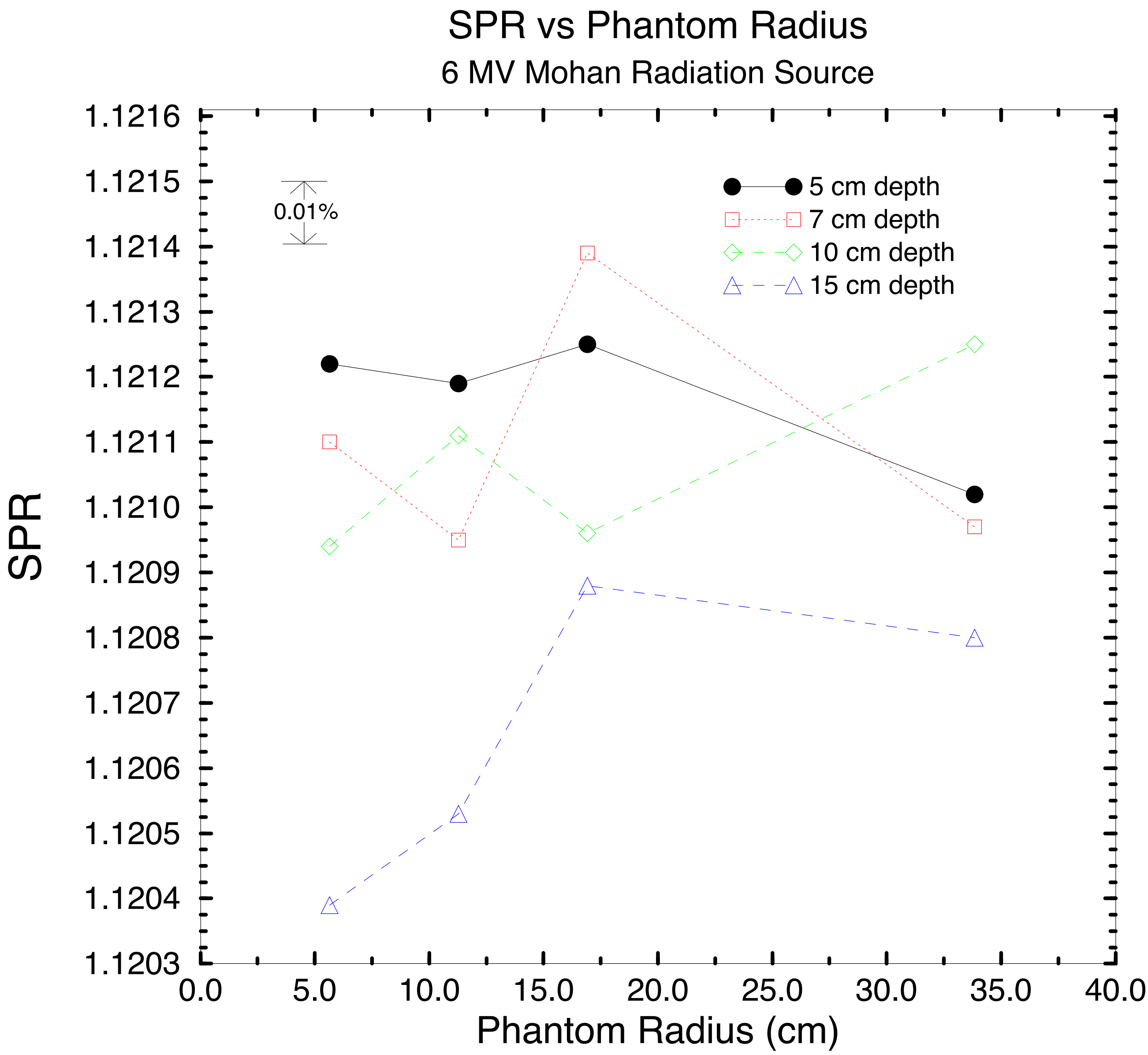

Figure 5: SPR vs phantom radius for 6 MV Mohan source

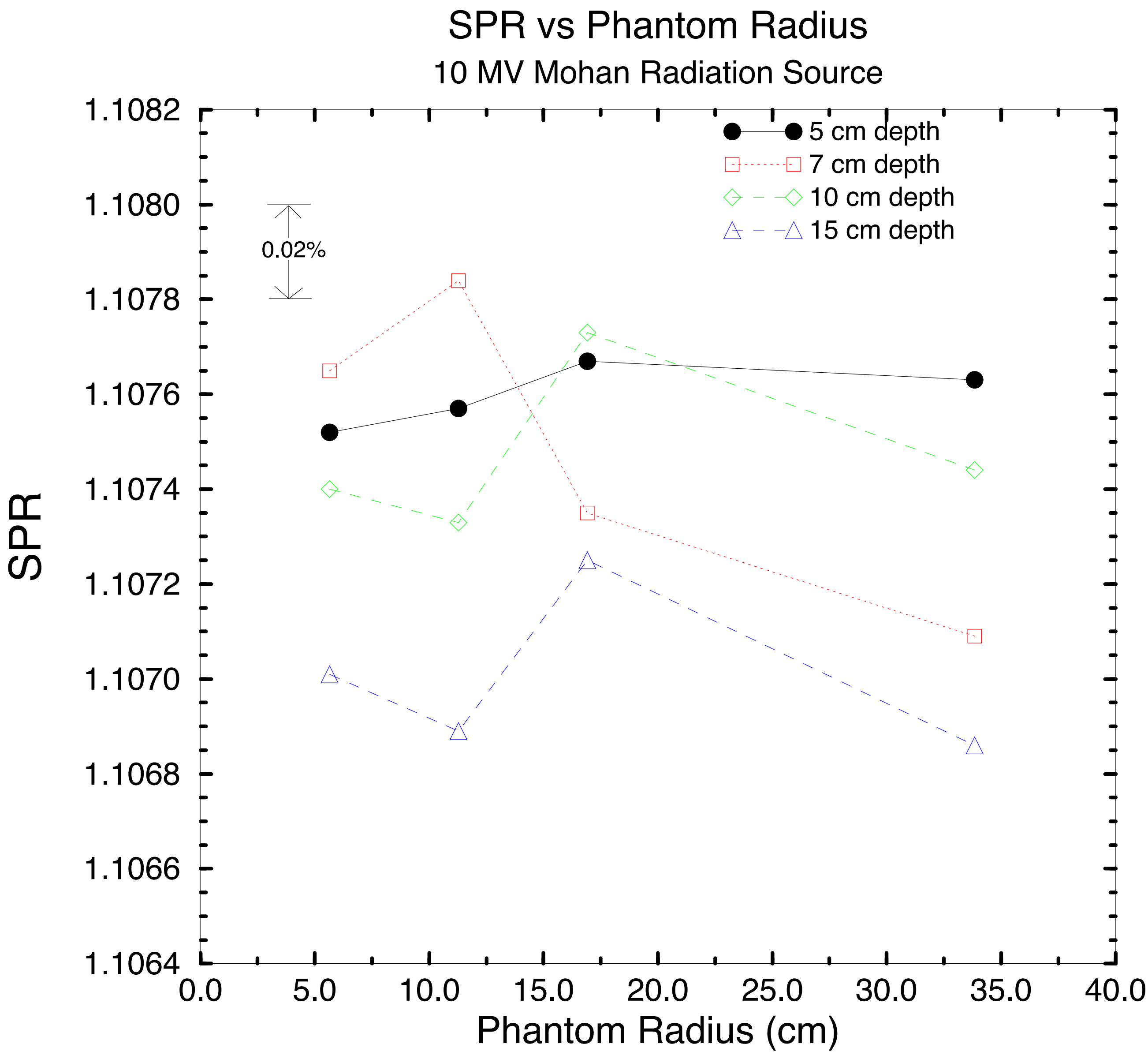

Figure 6: SPR vs phantom radius for 10 MV Mohan source

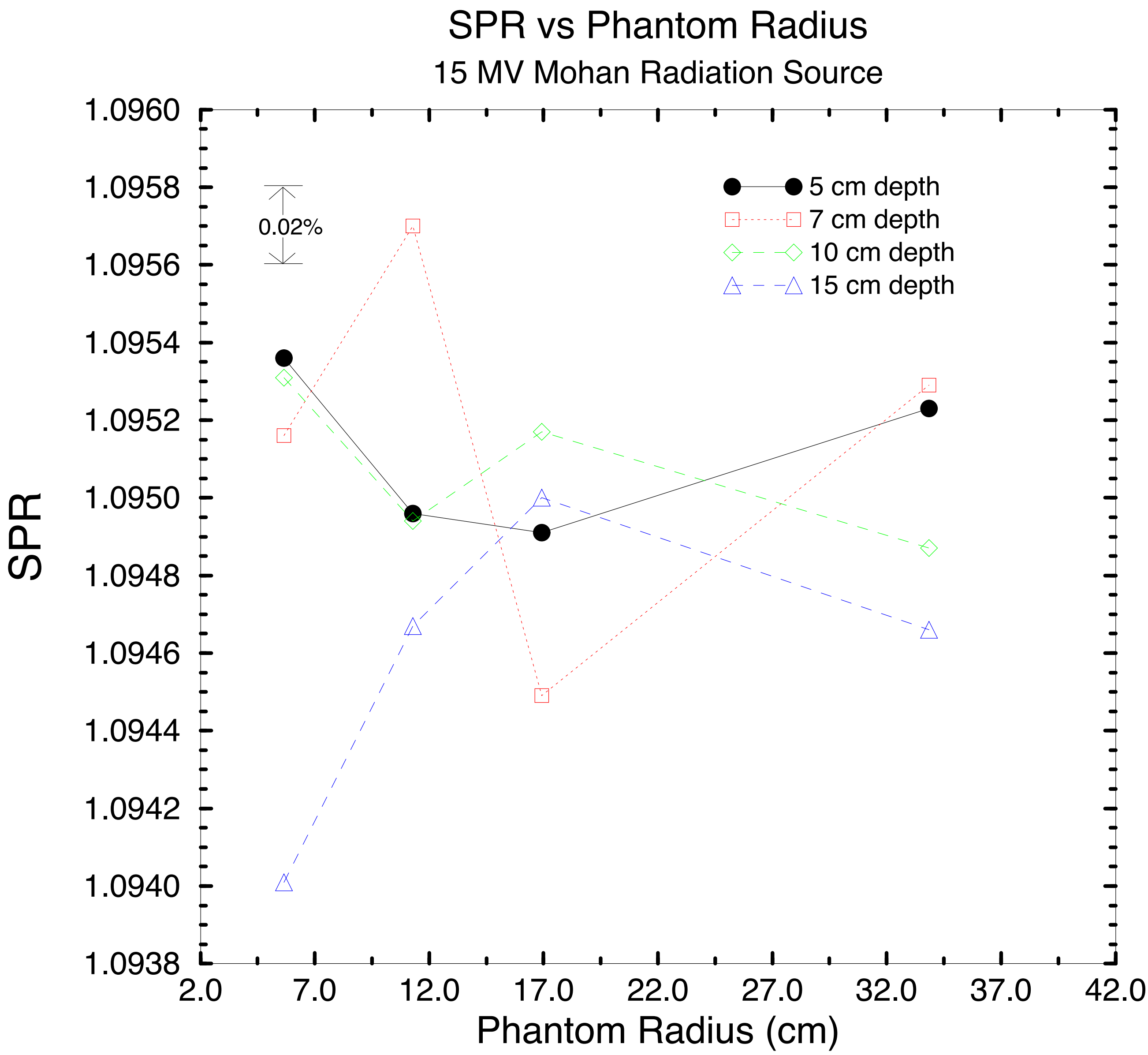

Figure 7: SPR vs phantom radius for 15 MV Mohan source

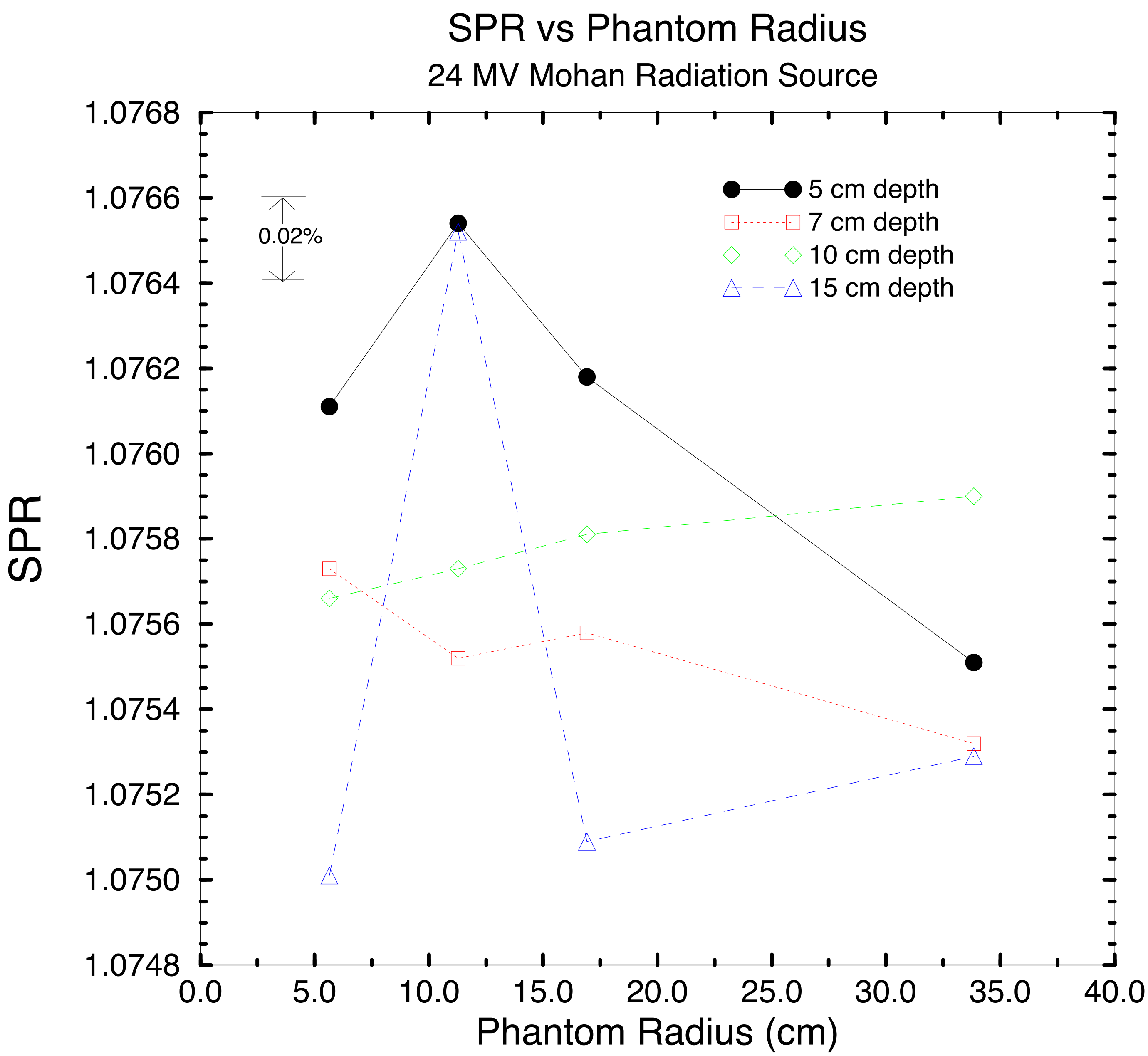

Figure 8: SPR vs phantom radius for 24 MV Mohan source

3 SPR vs Radial Position at Fixed Depths

The following graphs illustrate how the SPR varies in the radial direction for depths of 5 cm, 7 cm, 10 cm, and 15 cm. The plots are made out to a radial distance of 5.6 cm which is the radius of the incident beam in all cases. Each plot is for a specified depth and radiation source.

3.1 ^{60}Co Source

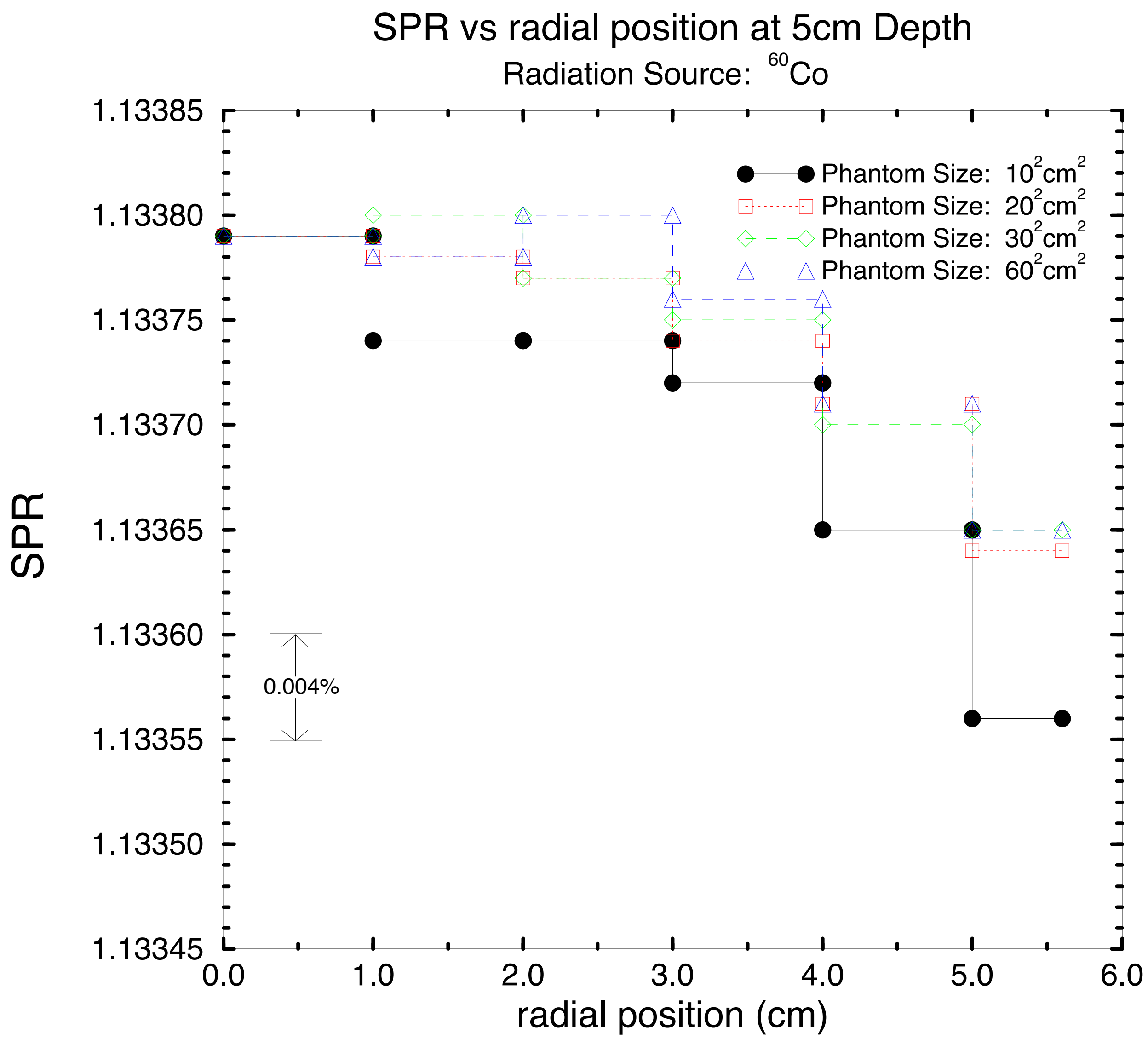

Figure 9: SPR vs radial position at 5 cm depth

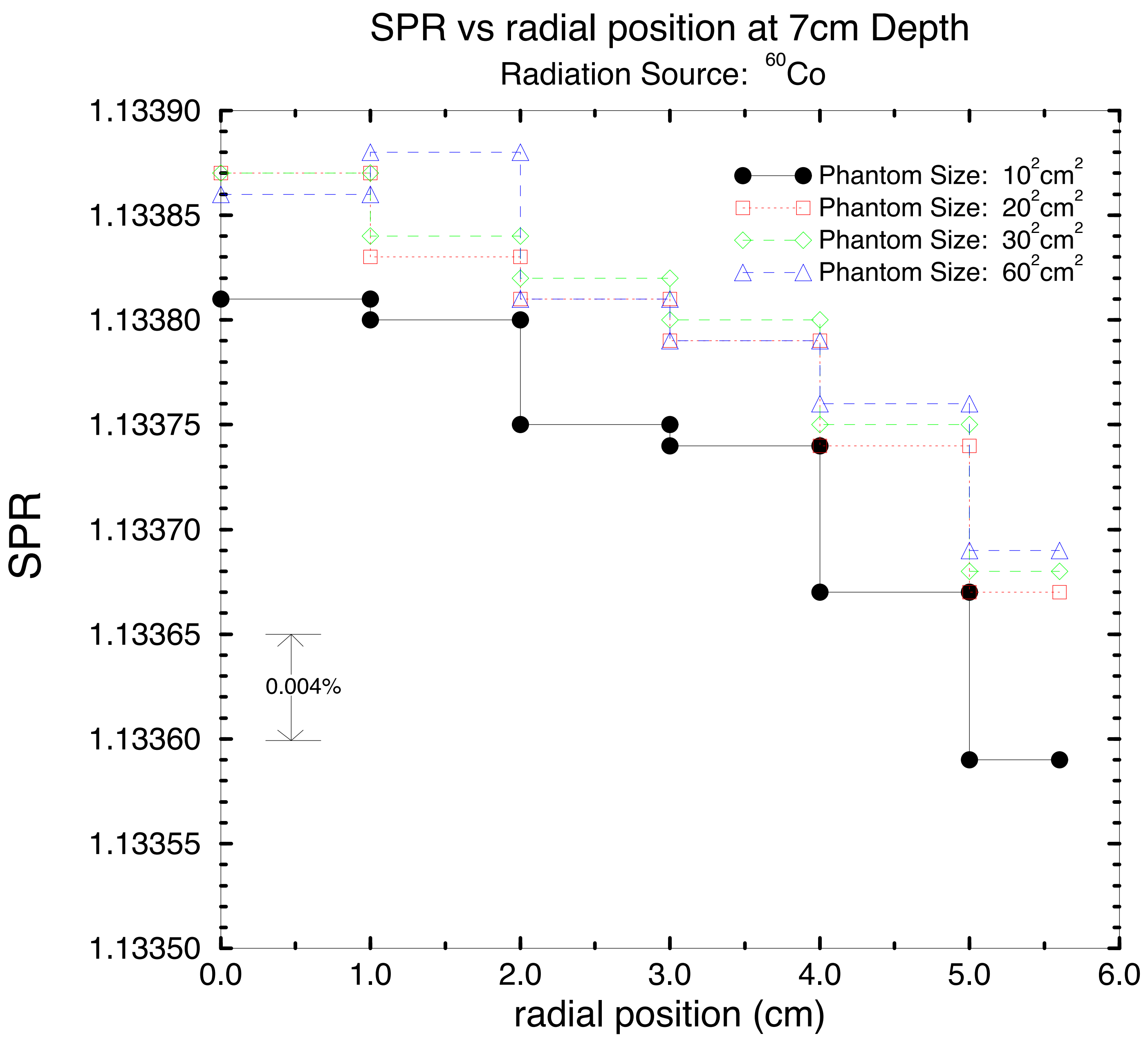

Figure 10: SPR vs radial position at 7 cm depth

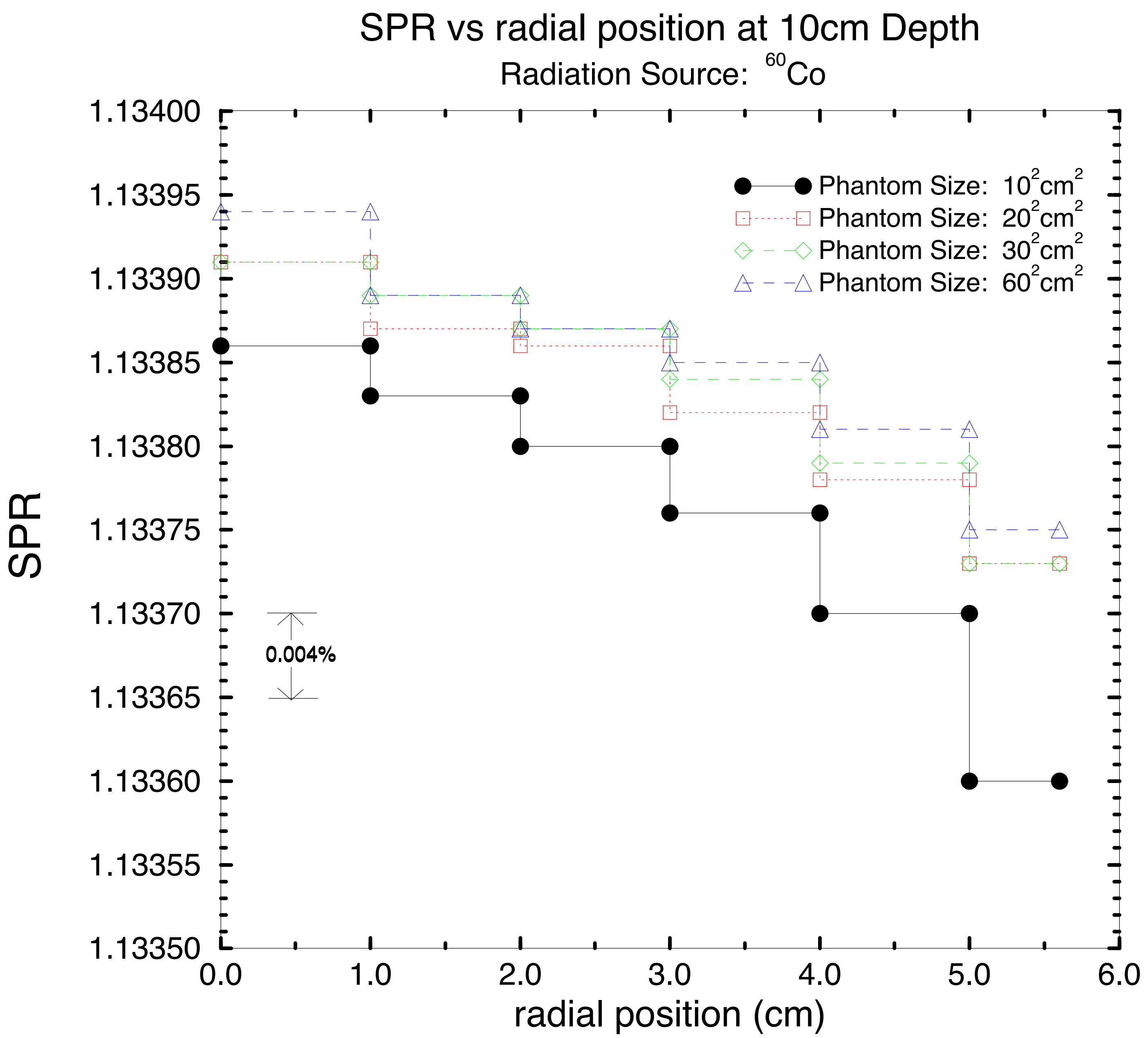

Figure 11: SPR vs radial position at 10 cm depth

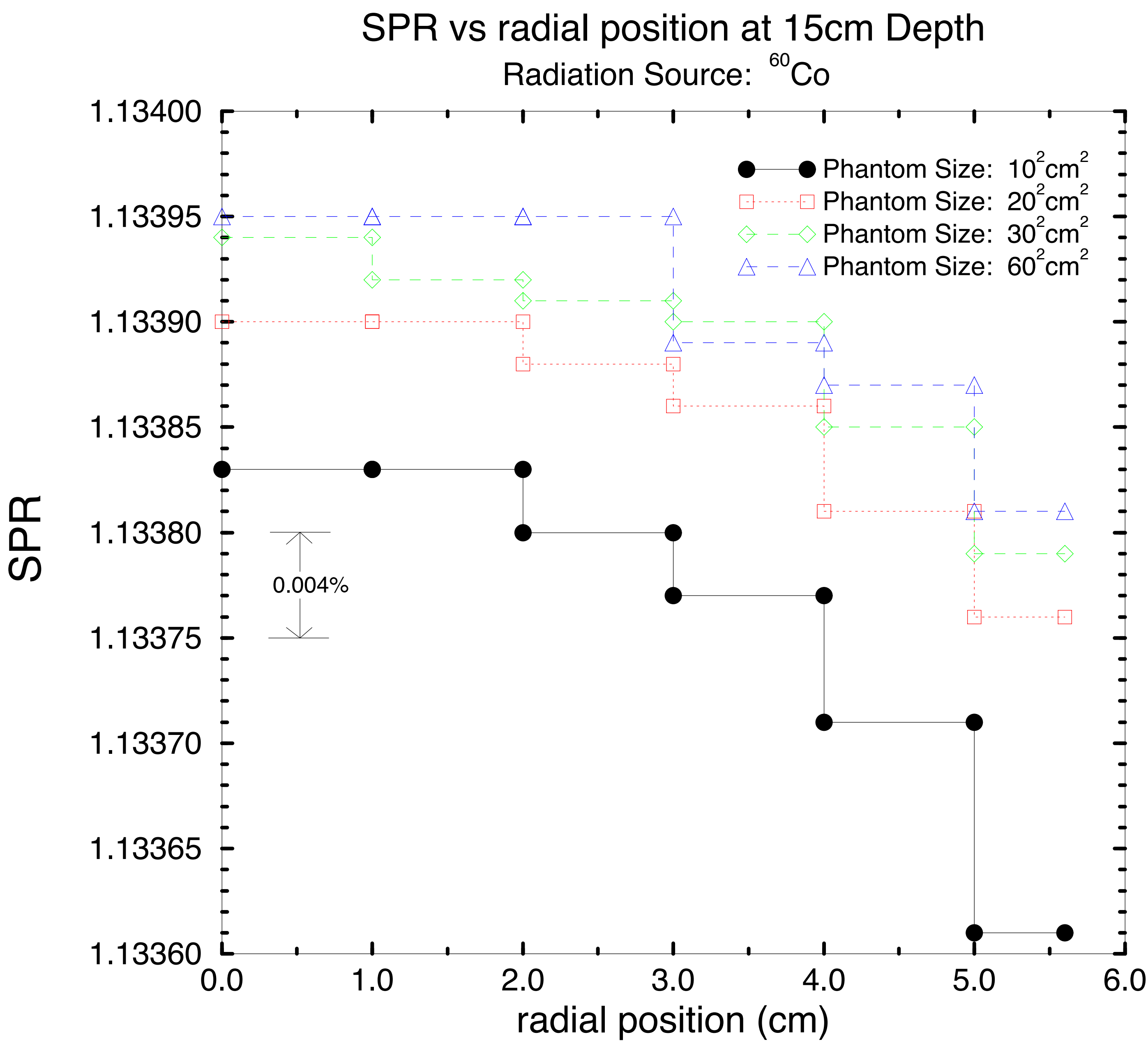

Figure 12: SPR vs radial position at 15 cm depth

3.2 4 MV Source

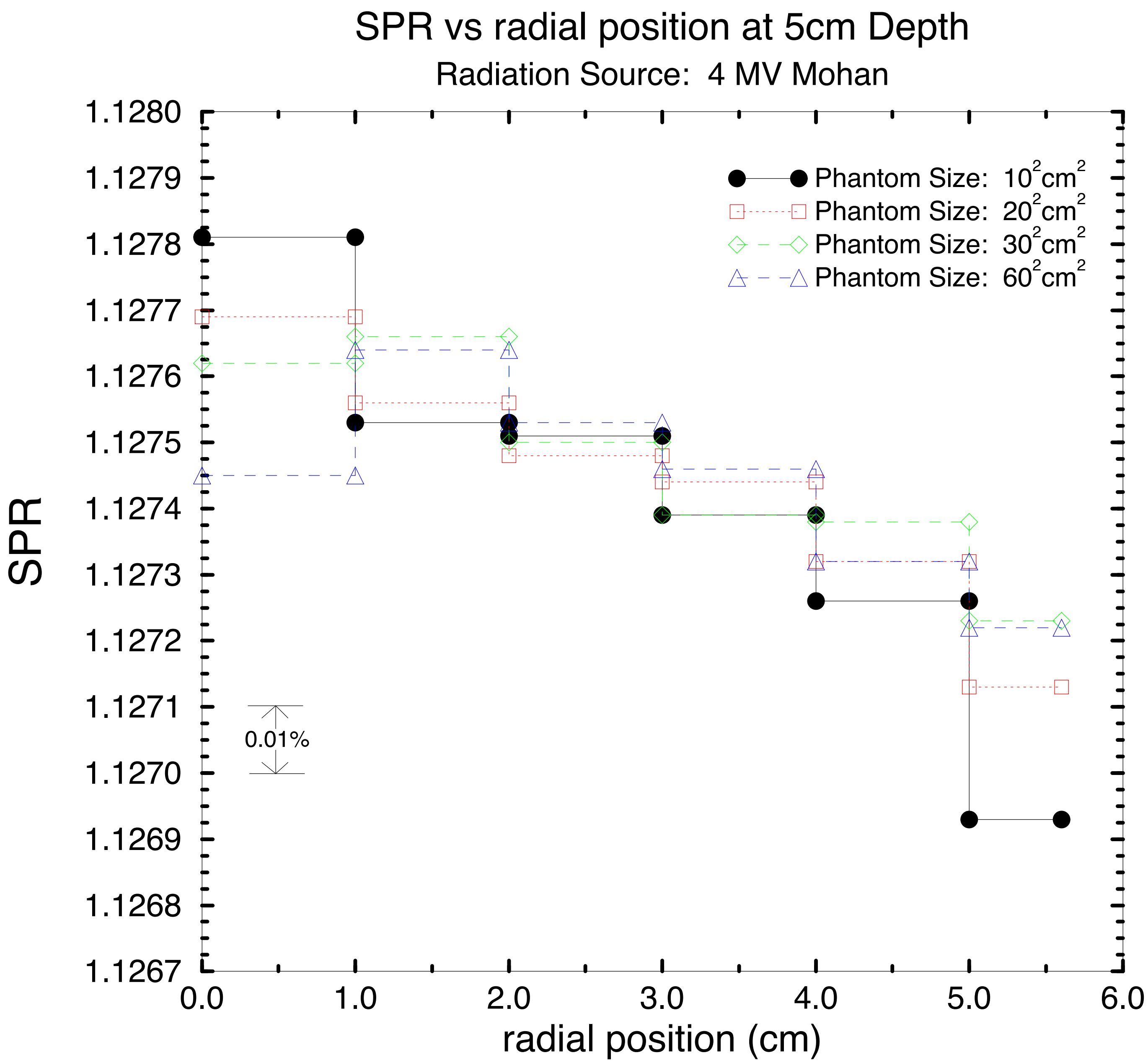

Figure 13: SPR vs radial position at 5 cm depth

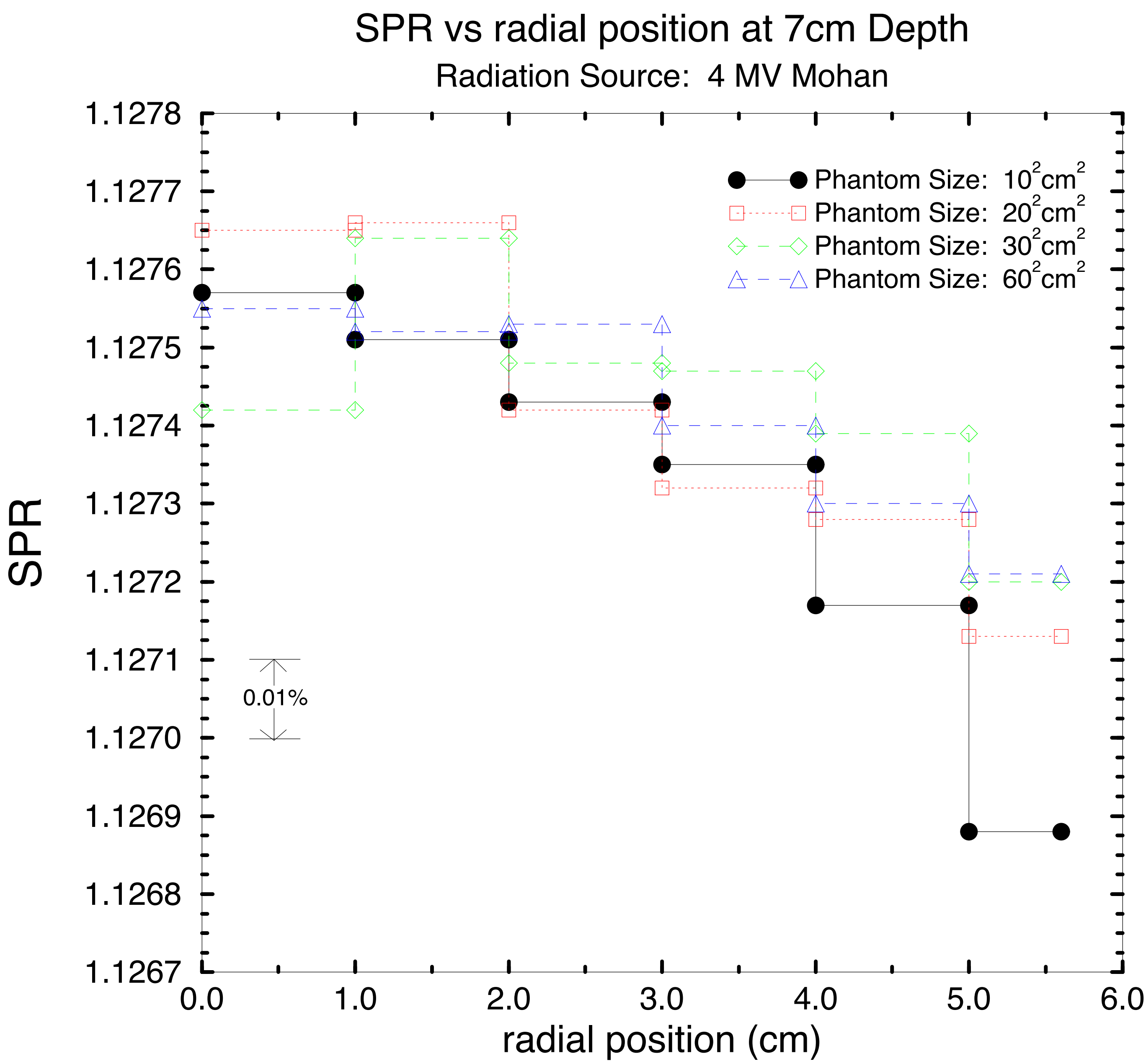

Figure 14: SPR vs radial position at 7 cm depth

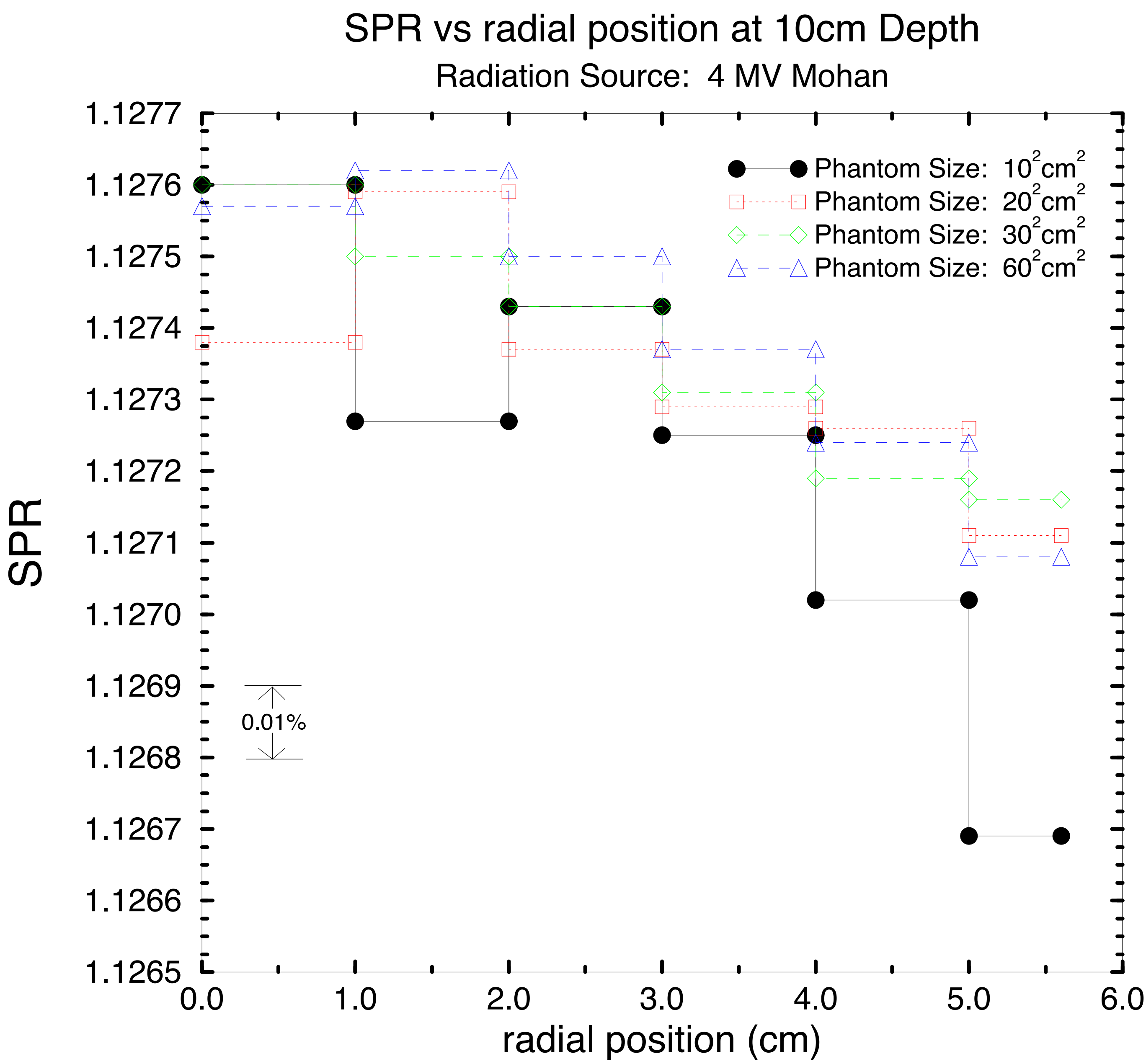

Figure 15: SPR vs radial position at 10 cm depth

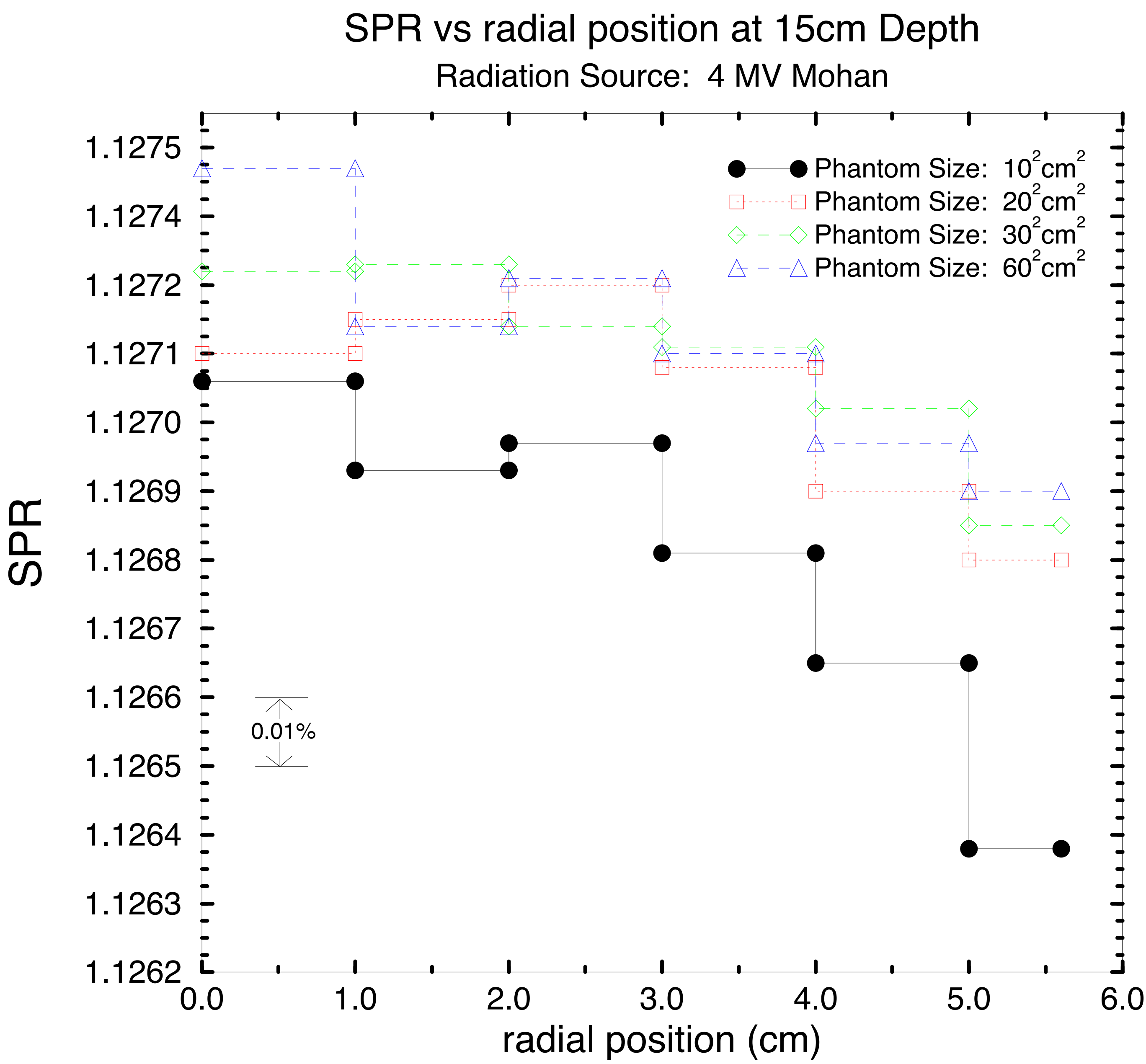

Figure 16: SPR vs radial position at 15 cm depth

3.3 6 MV Source

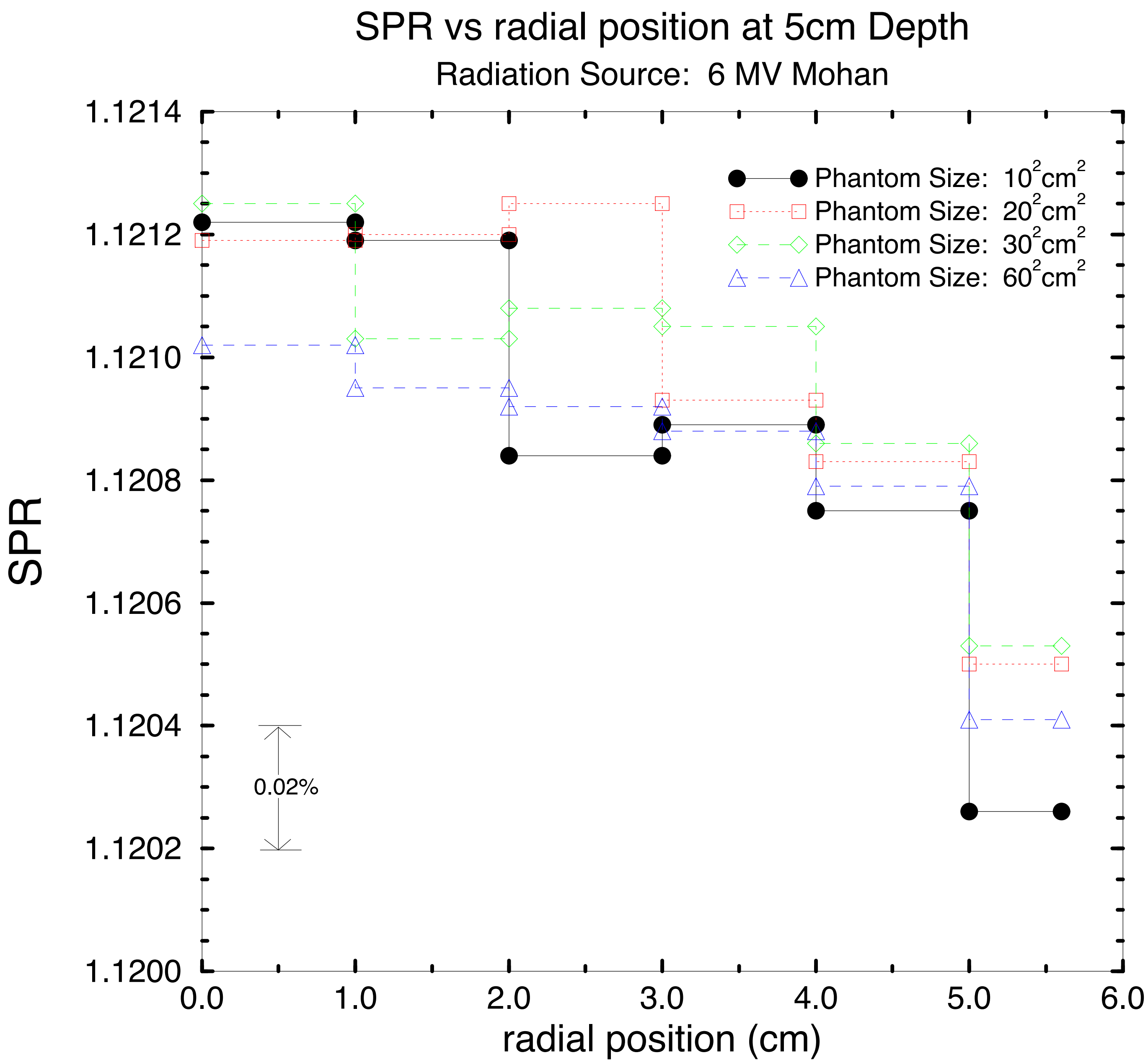

Figure 17: SPR vs radial position at 5 cm depth

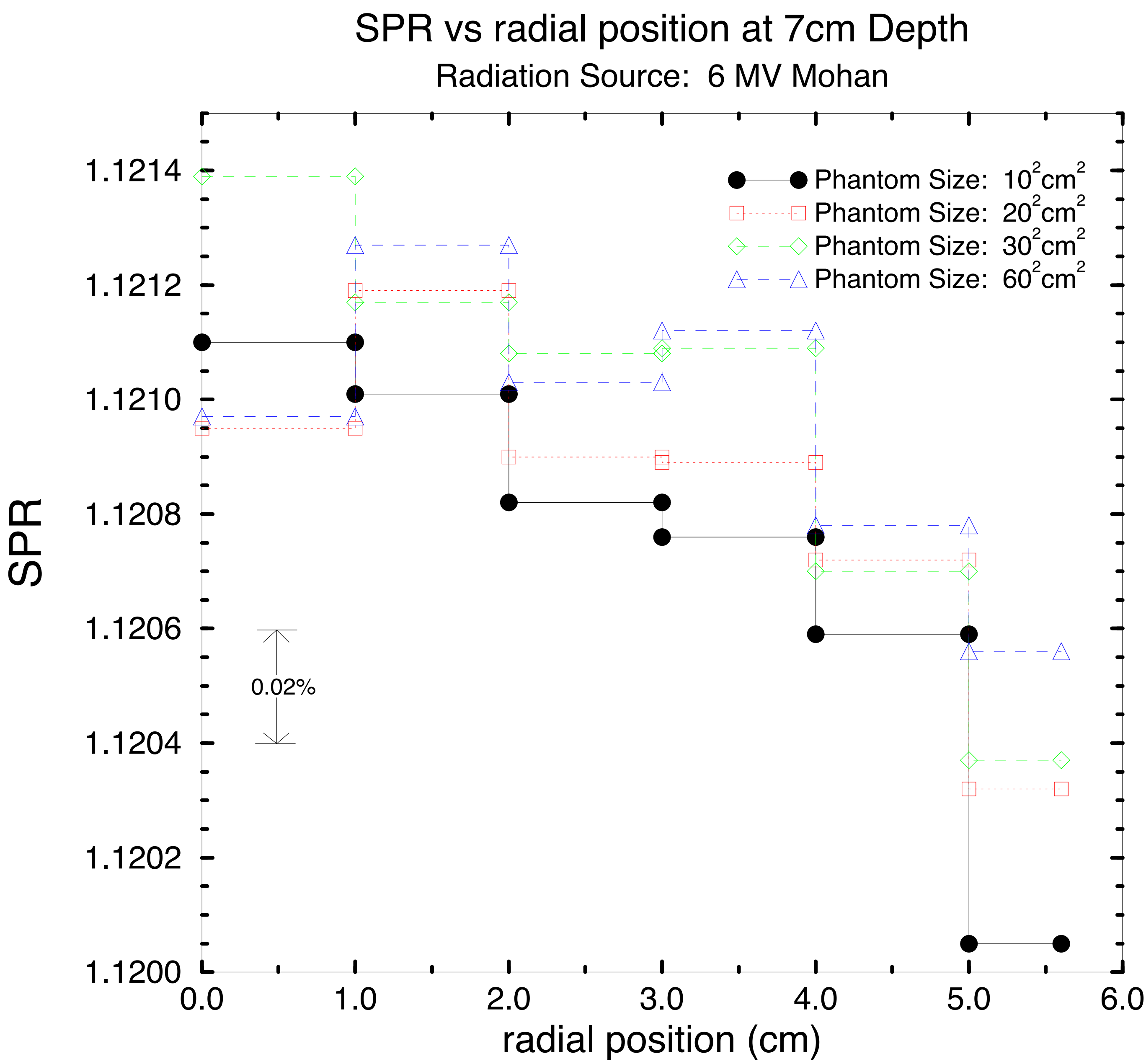

Figure 18: SPR vs radial position at 7 cm depth

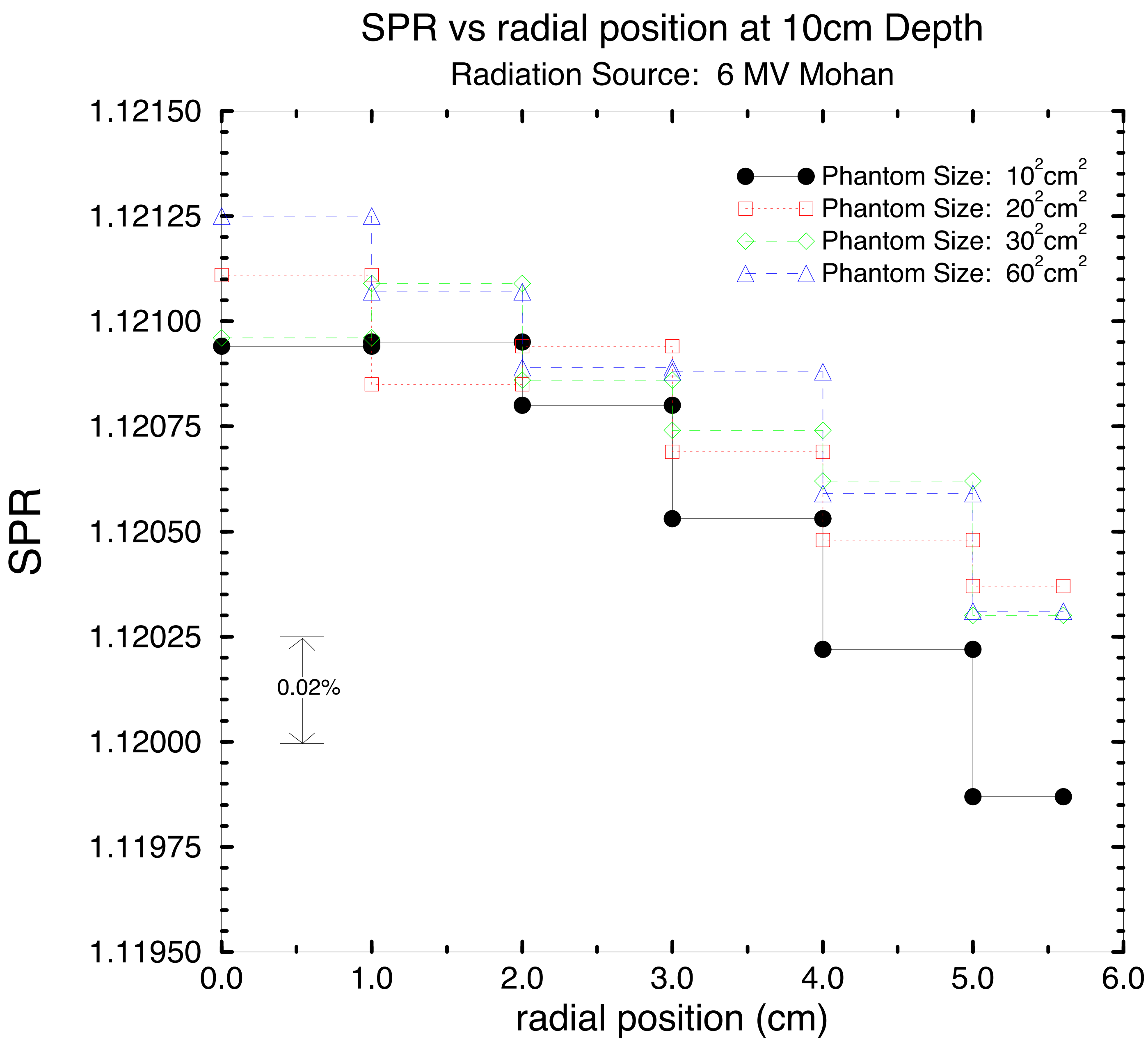

Figure 19: SPR vs radial position at 10 cm depth

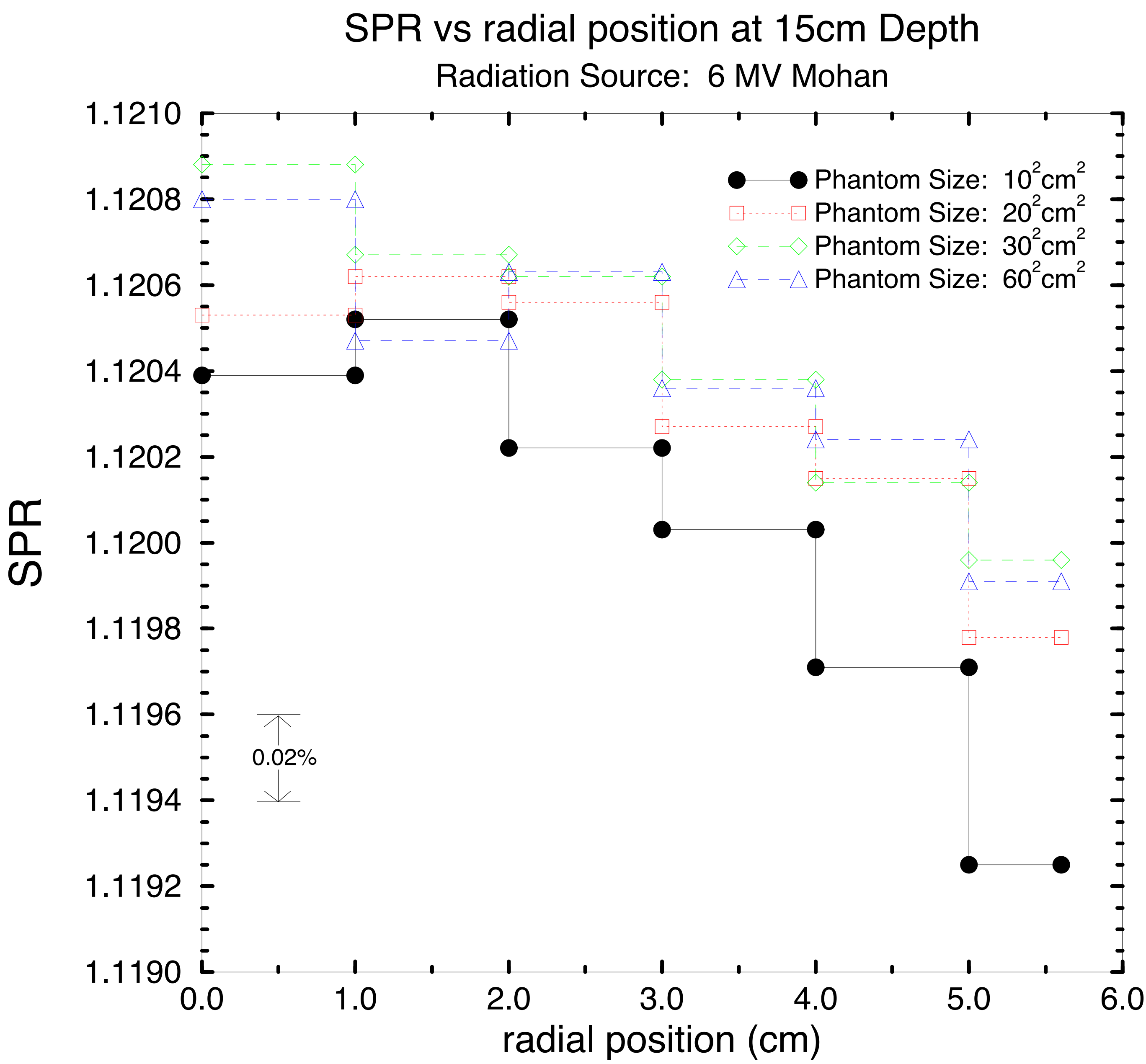

Figure 20: SPR vs radial position at 15 cm depth

3.4 10 MV Source

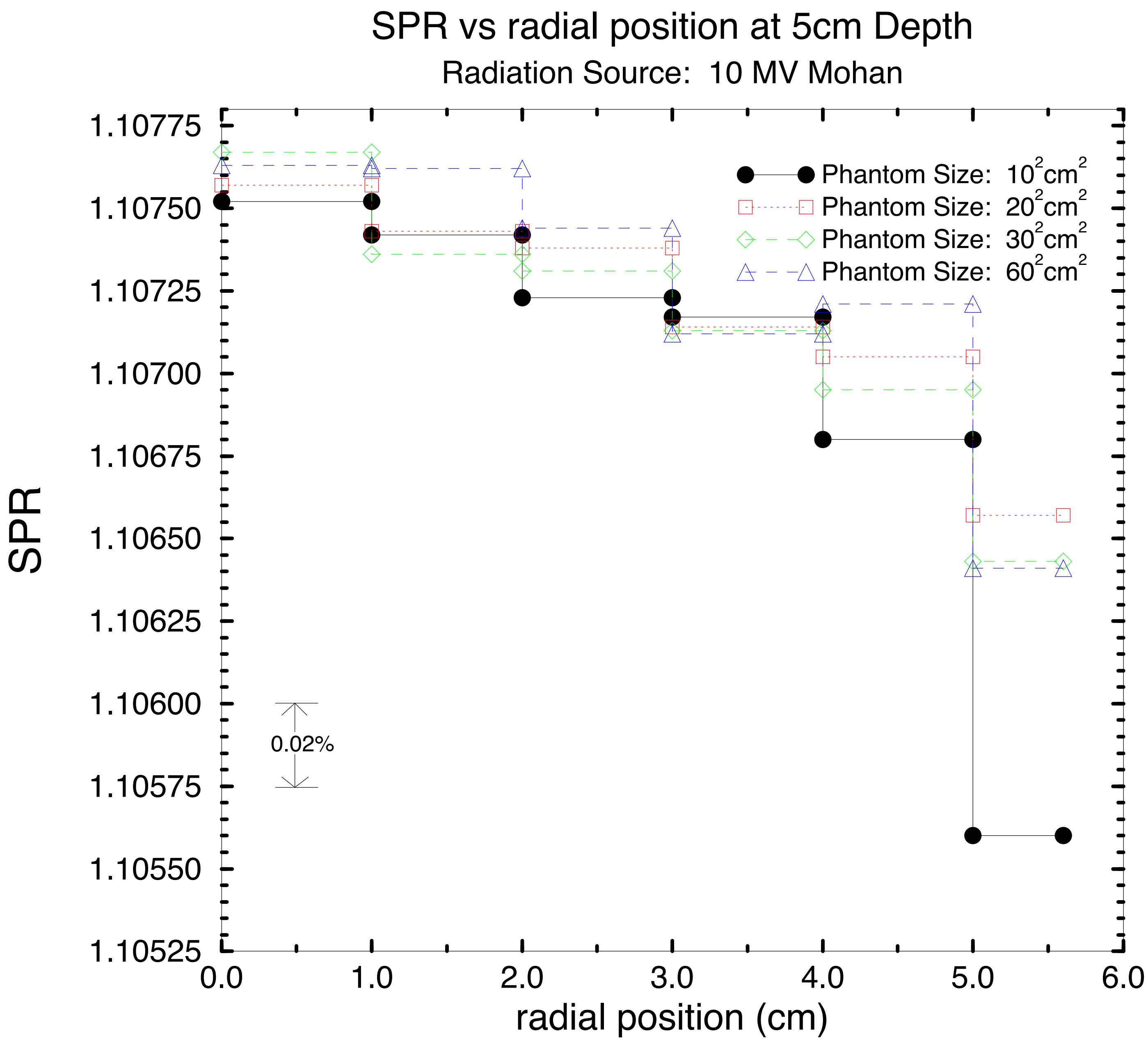

Figure 21: SPR vs radial position at 5 cm depth

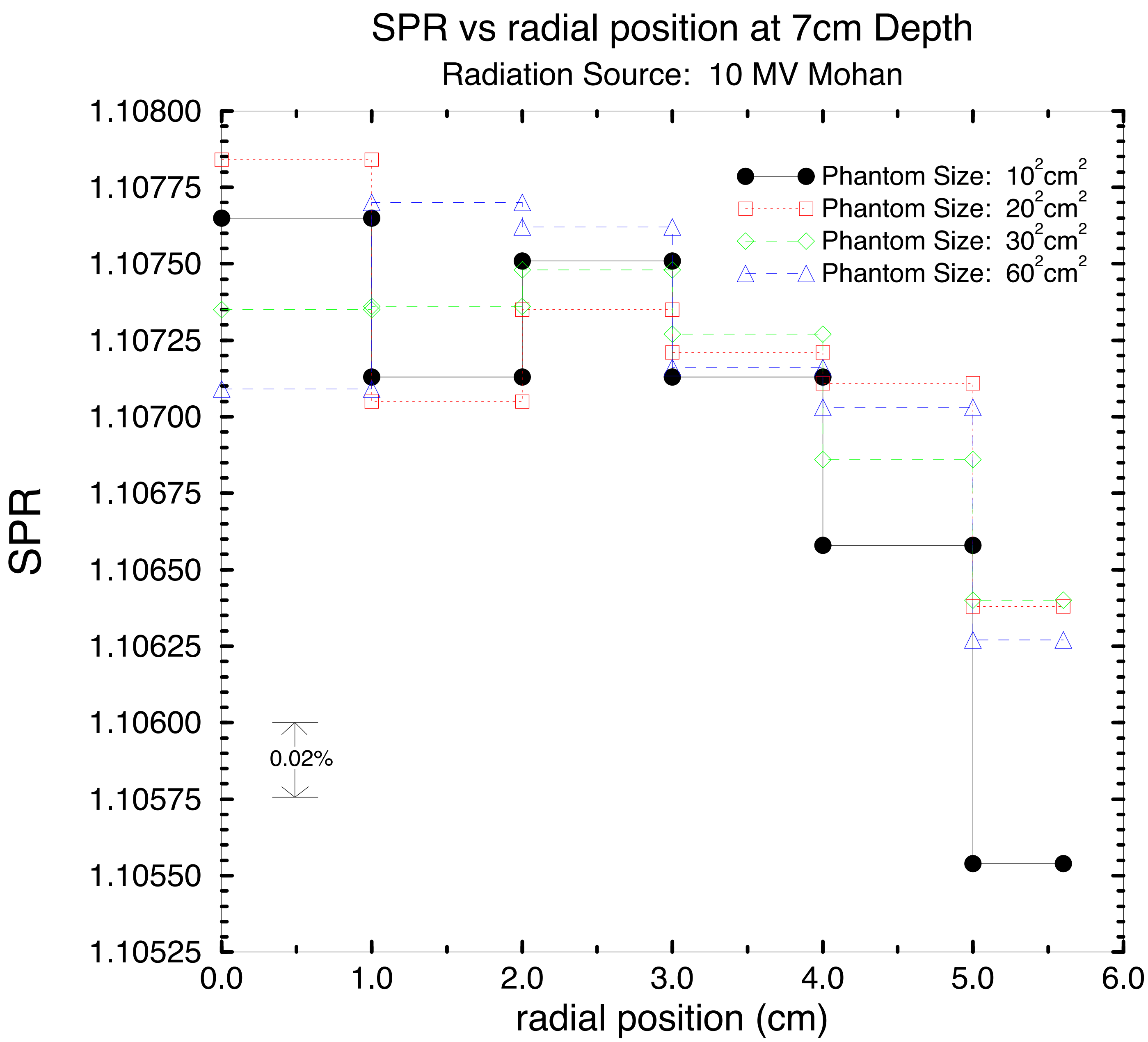

Figure 22: SPR vs radial position at 7 cm depth

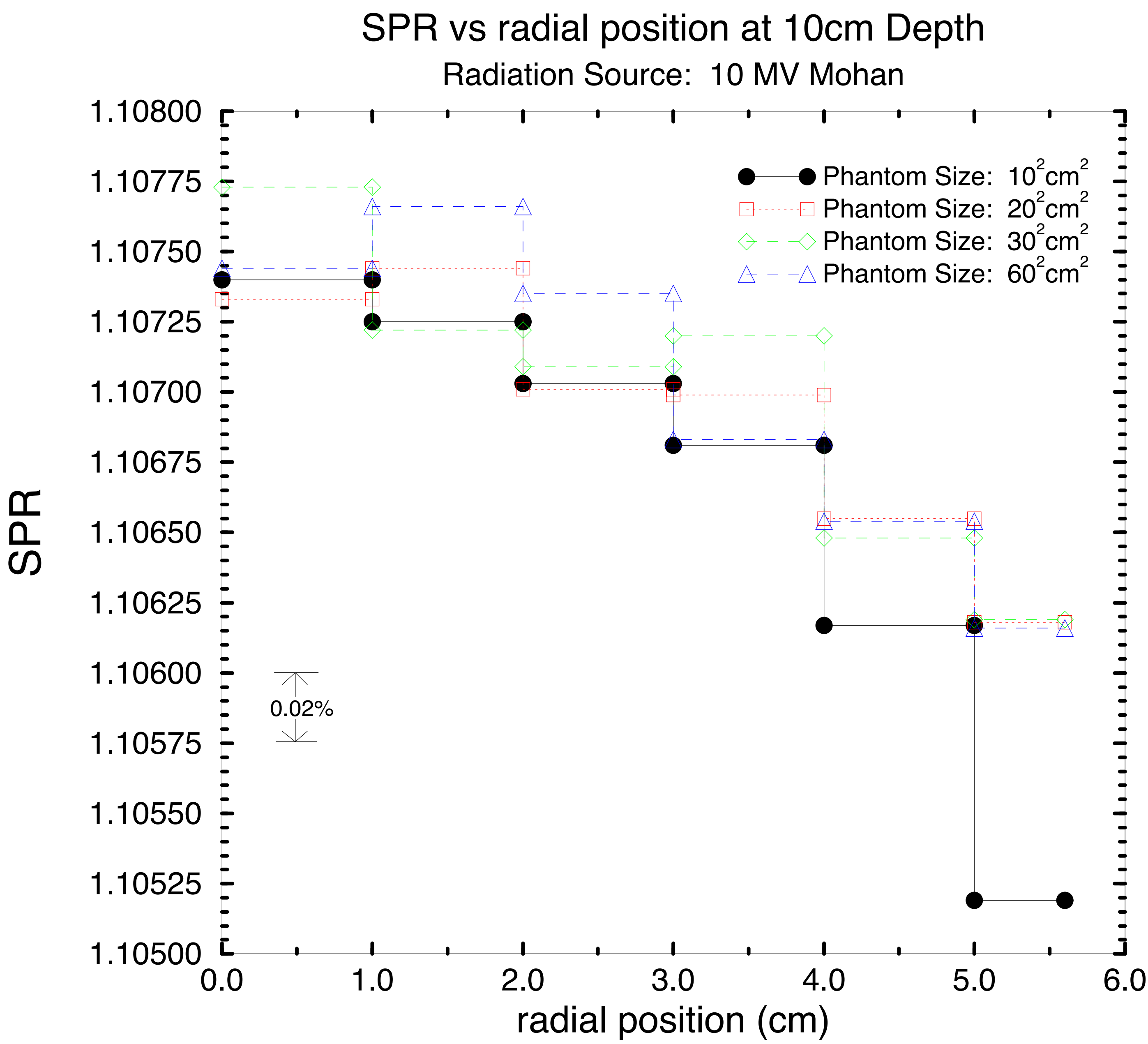

Figure 23: SPR vs radial position at 10 cm depth

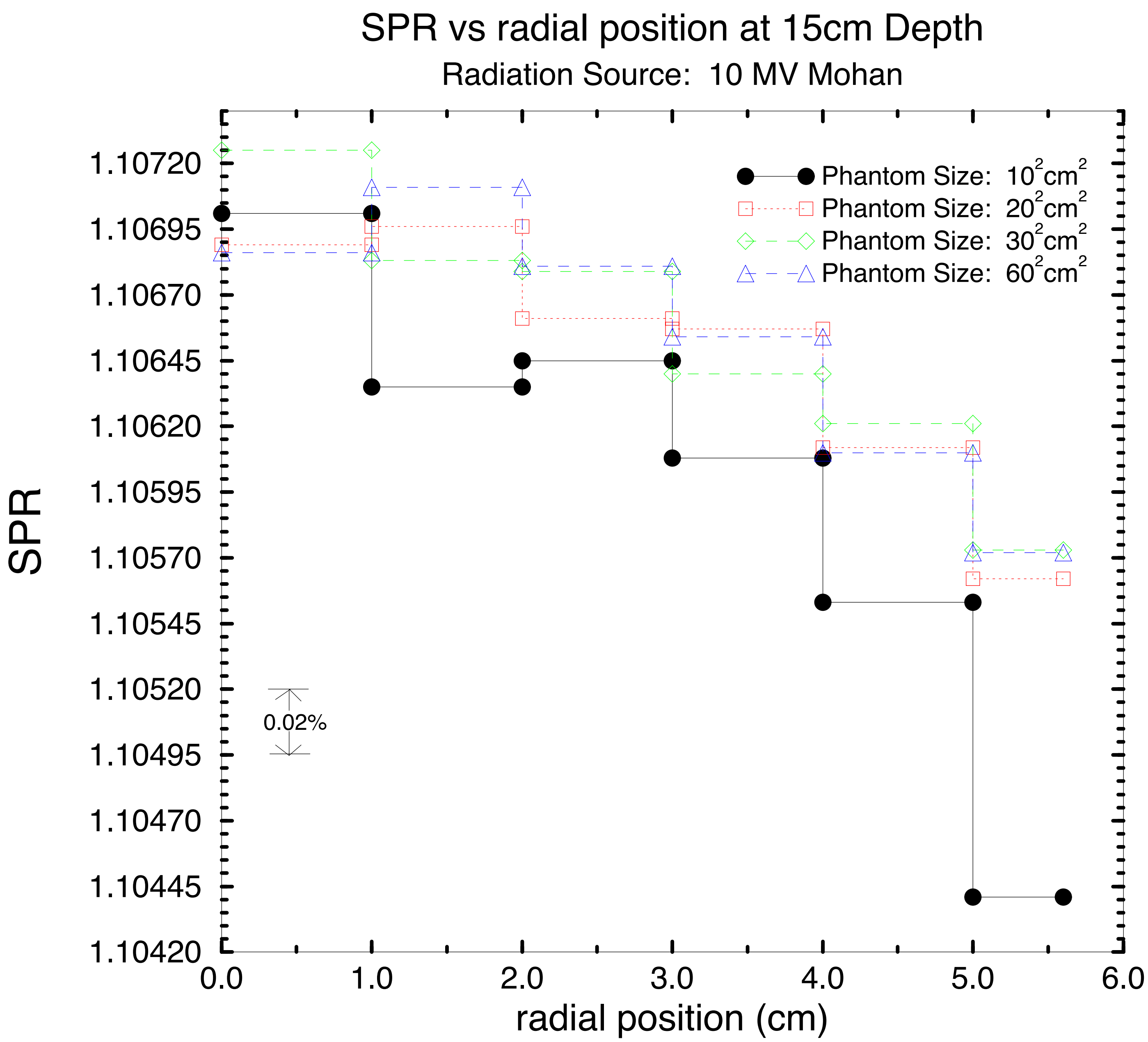

Figure 24: SPR vs radial position at 15 cm depth

3.5 15 MV Source

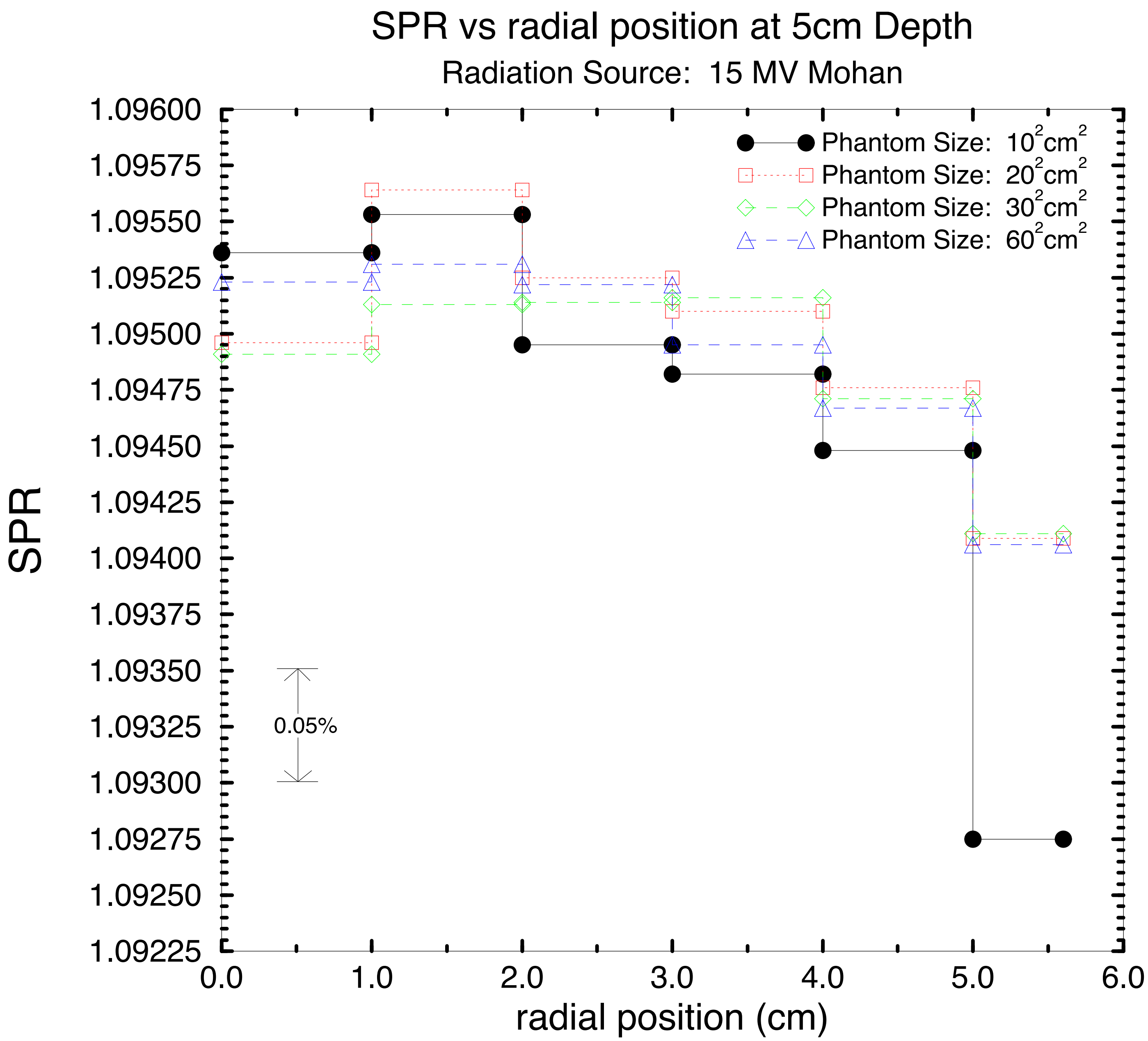

Figure 25: SPR vs radial position at 5 cm depth

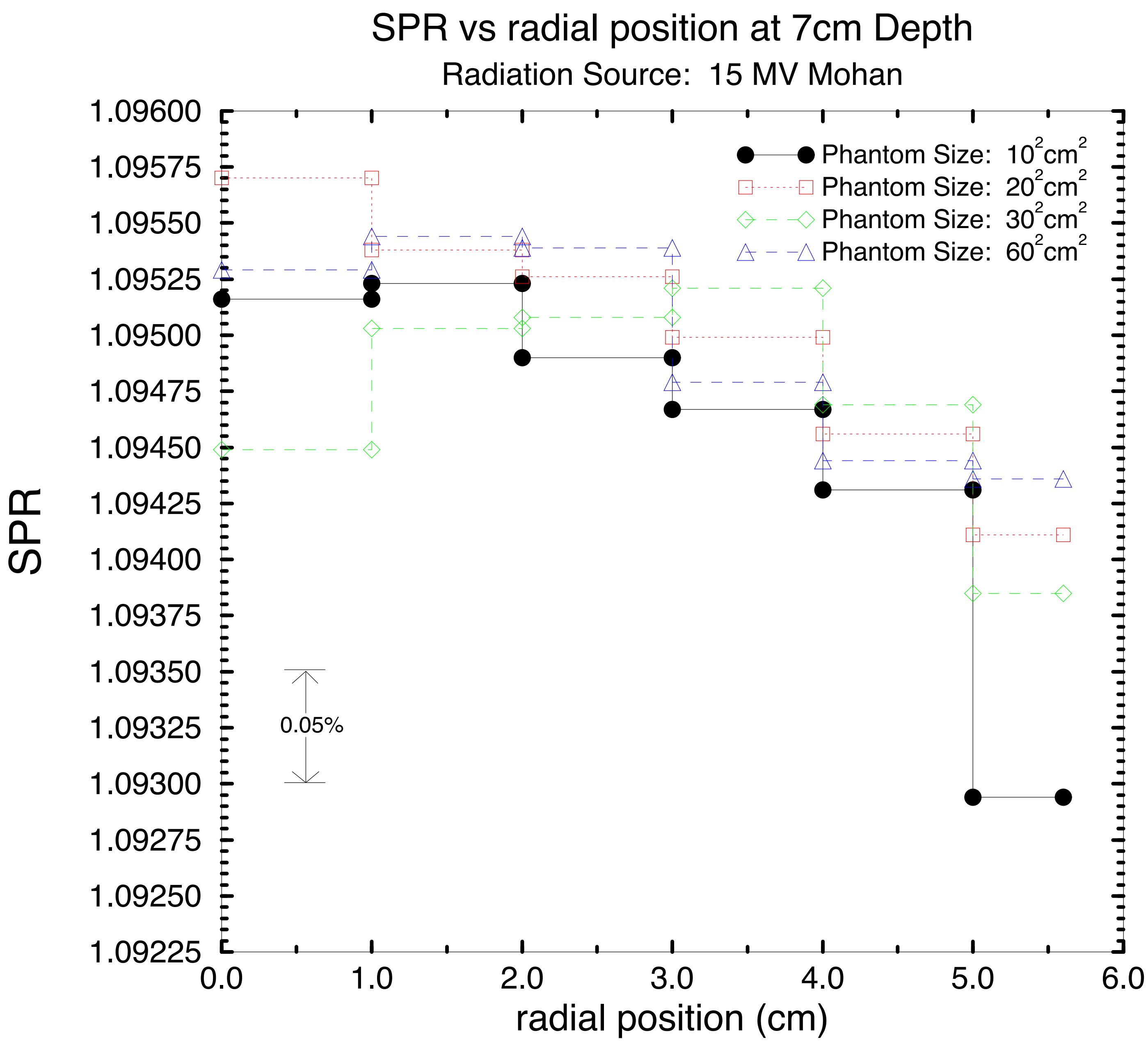

Figure 26: SPR vs radial position at 7 cm depth

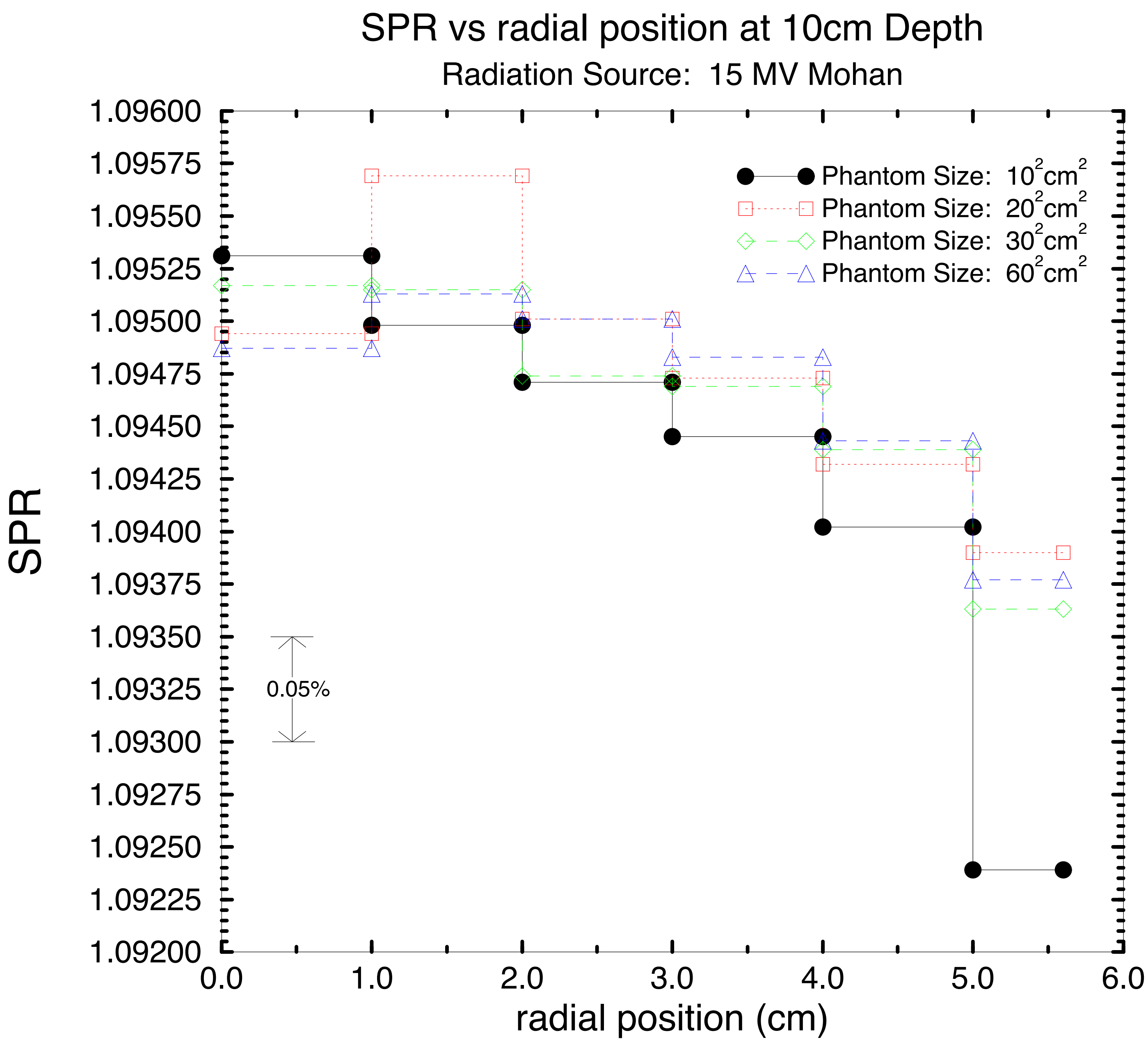

Figure 27: SPR vs radial position at 10 cm depth

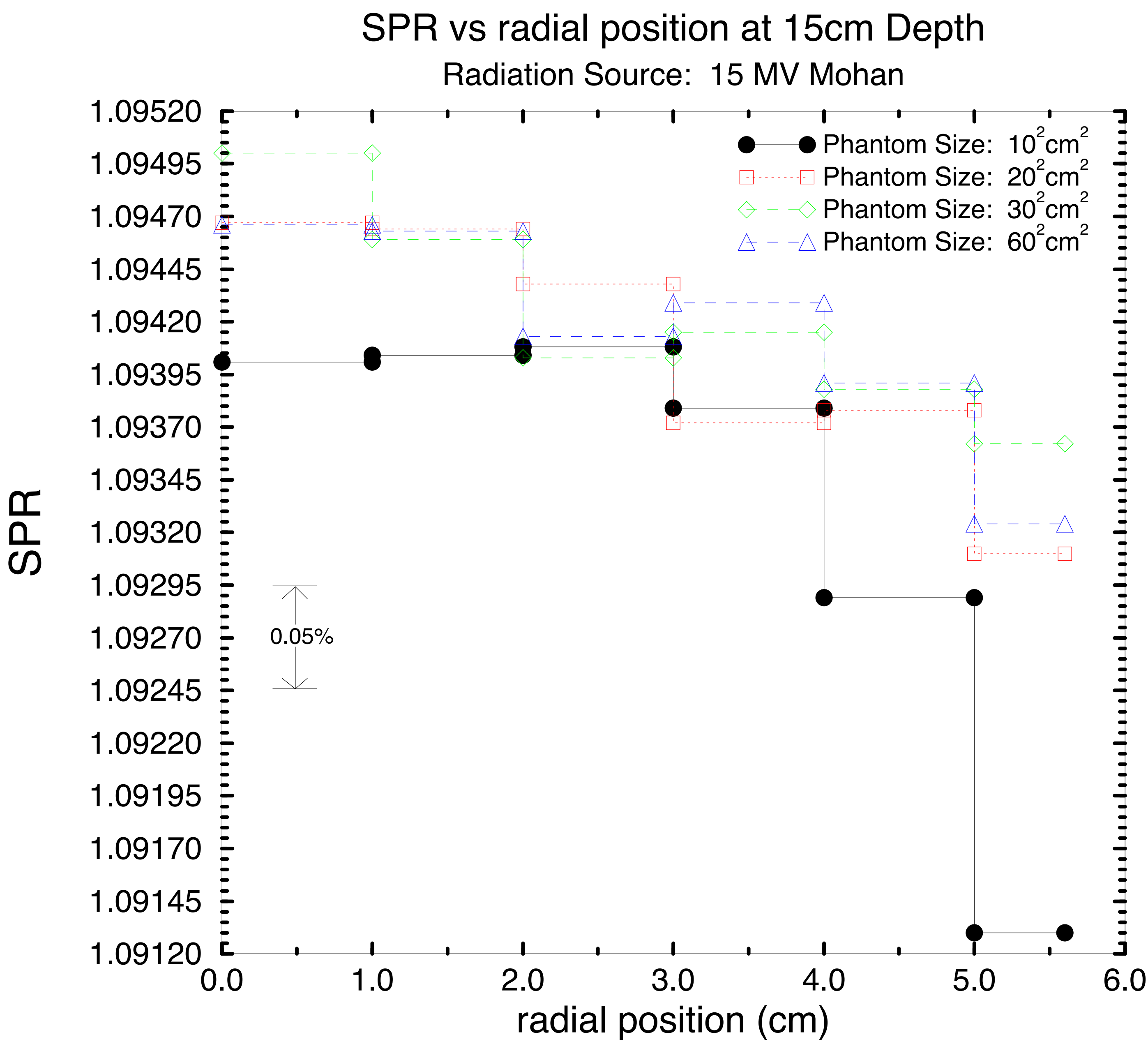

Figure 28: SPR vs radial position at 15 cm depth

3.6 24 MV Source

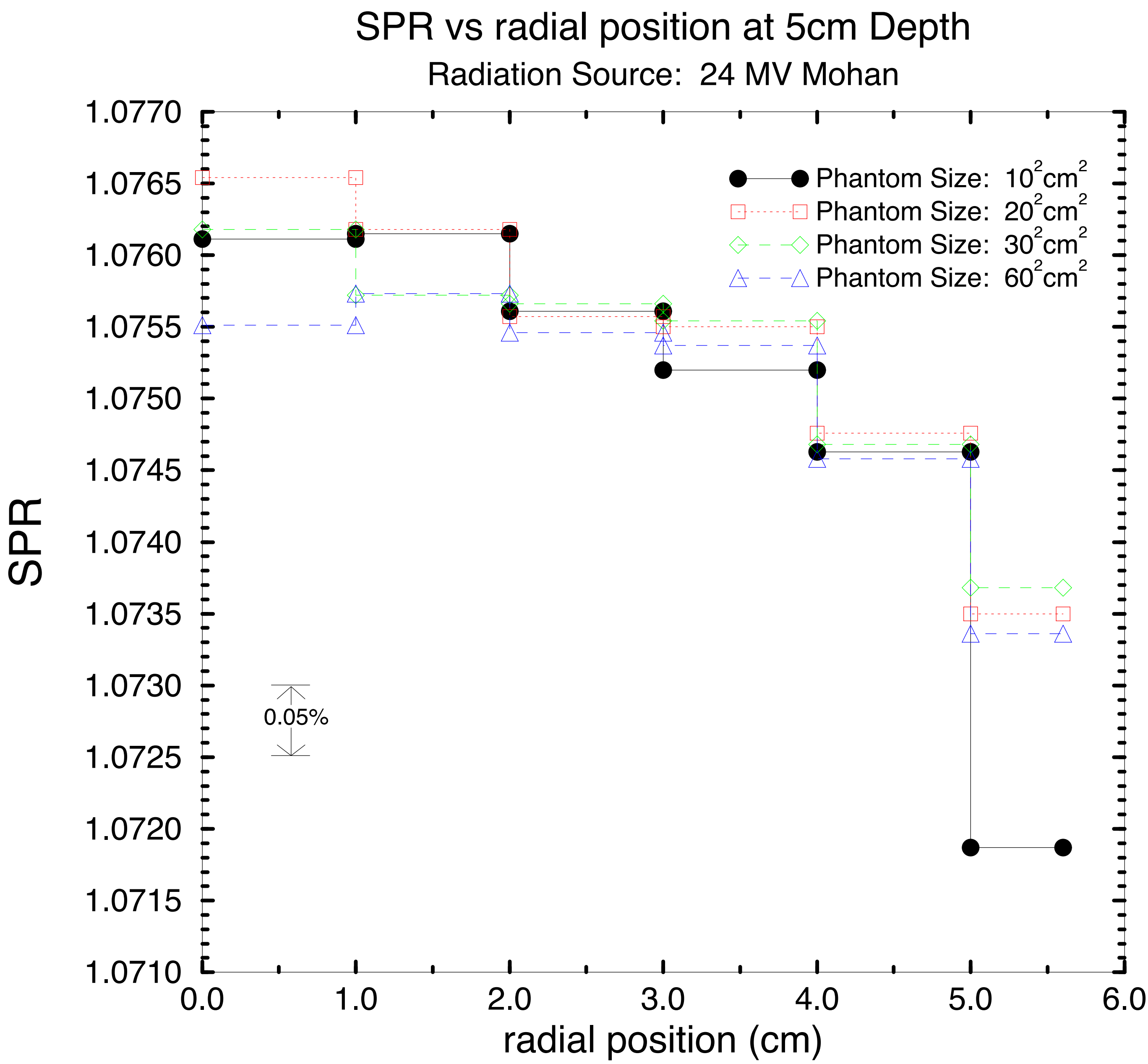

Figure 29: SPR vs radial position at 5 cm depth

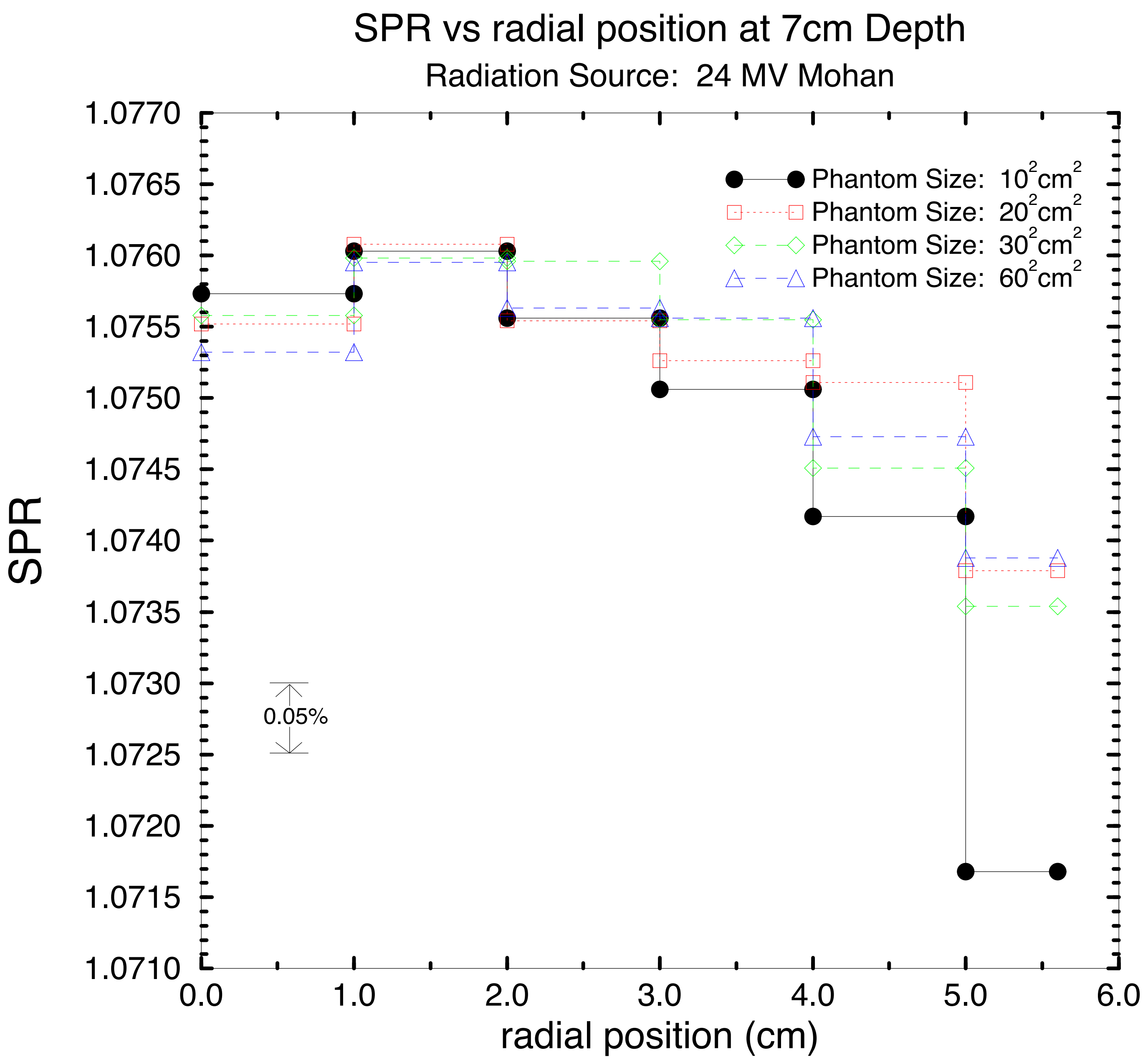

Figure 30: SPR vs radial position at 7 cm depth

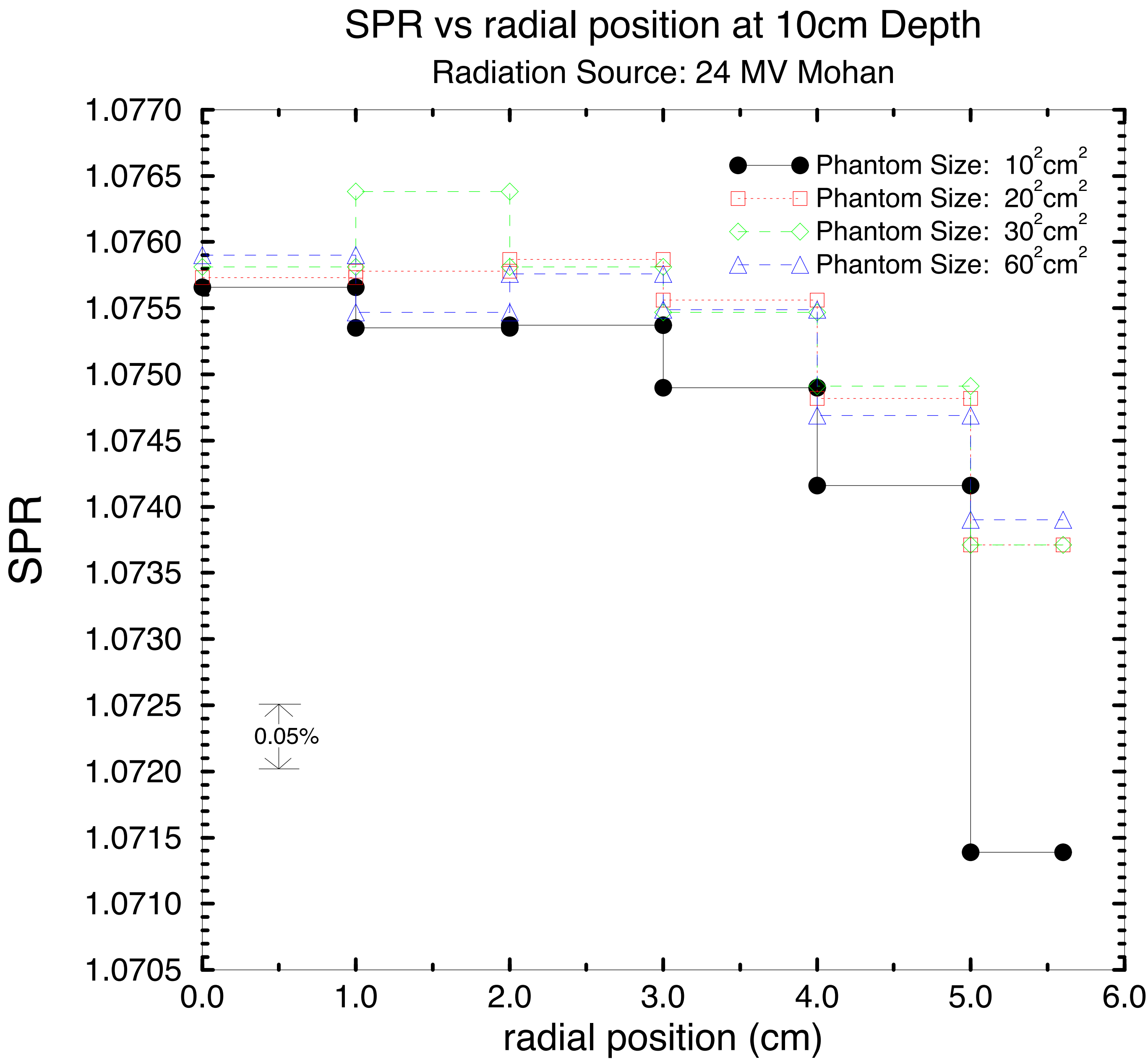

Figure 31: SPR vs radial position at 10 cm depth

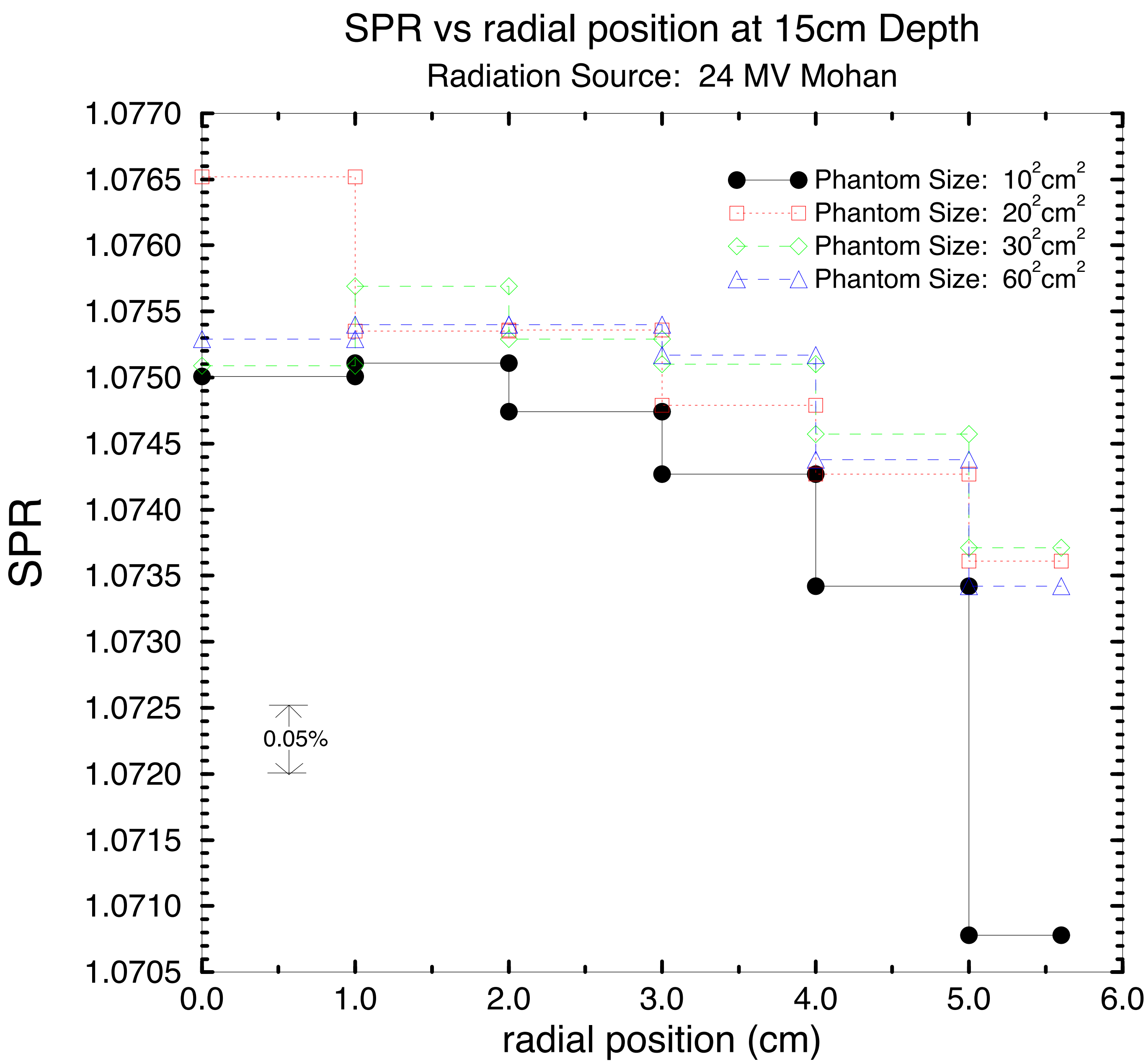

Figure 32: SPR vs radial position at 15 cm depth

4 SPR vs Depth

The following graphs show how the SPR varies with the depth in the phantom. The SPR data used for these graphs is from the inner most scoring region at each of the specified depths (ie. on the central axis). Each SPR data point has a statistical uncertainty of 0.02% or less.

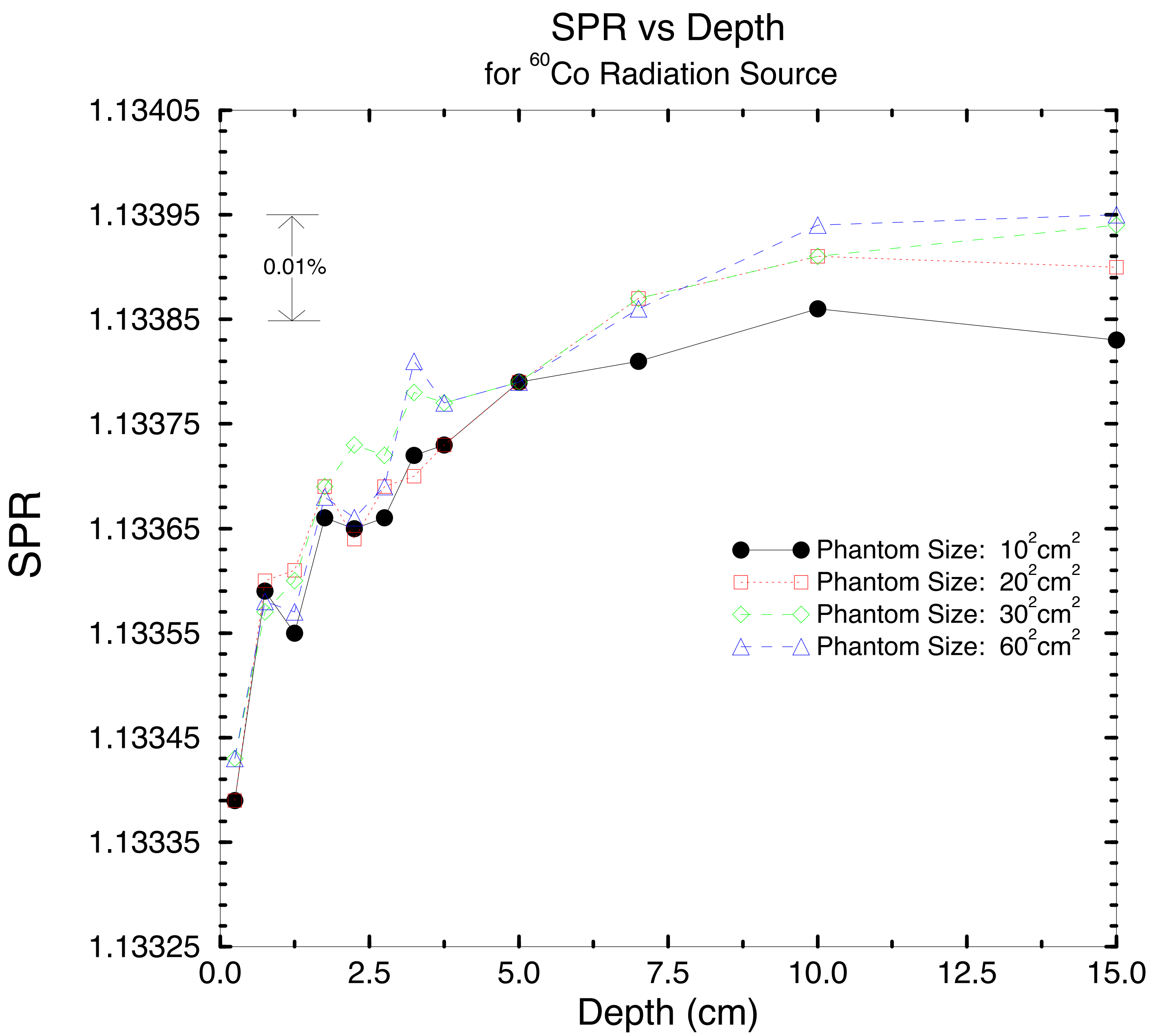

Figure 33: SPR vs depth for ^{60}Co source

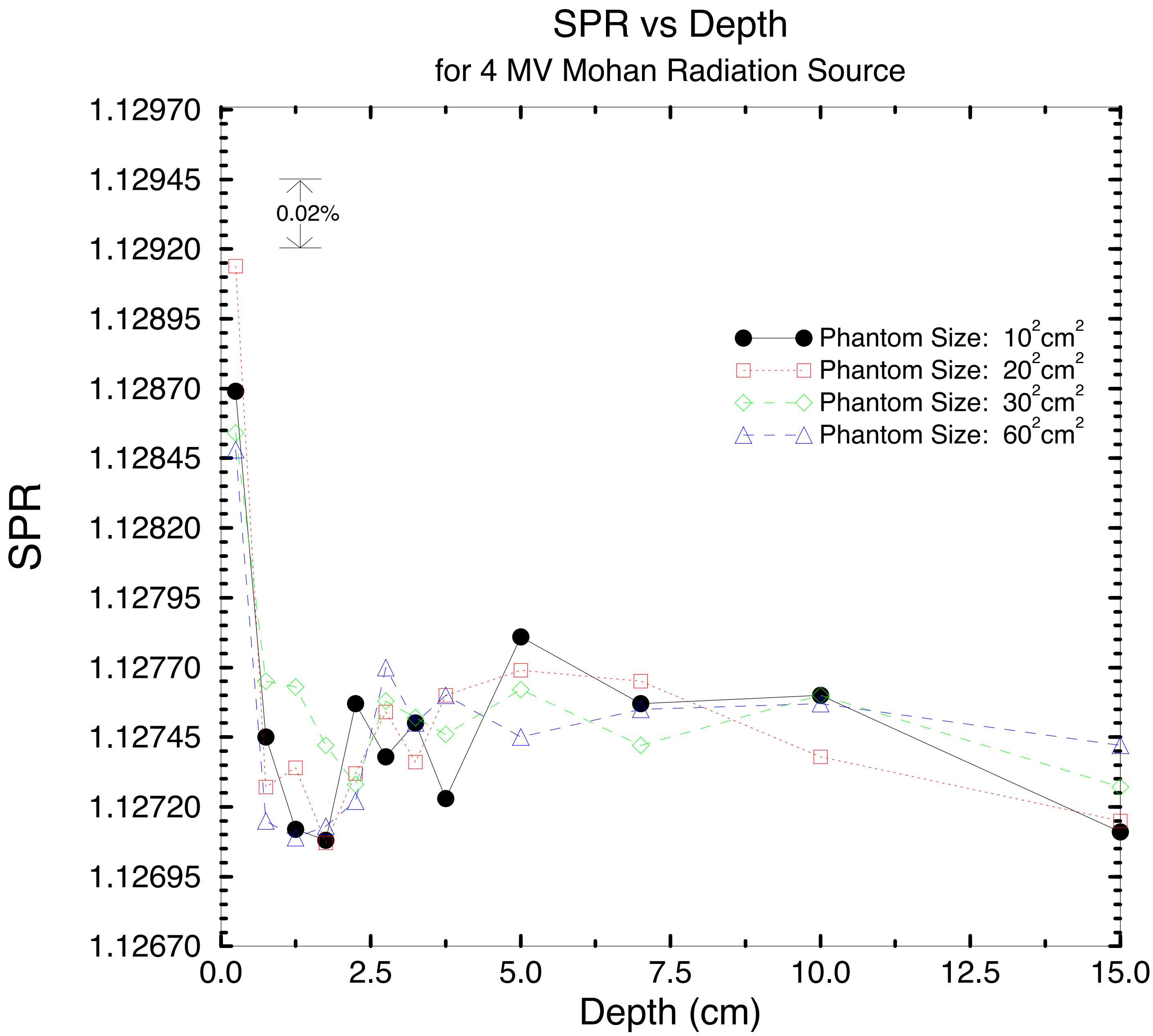

Figure 34: SPR vs depth for 4 MV Mohan source

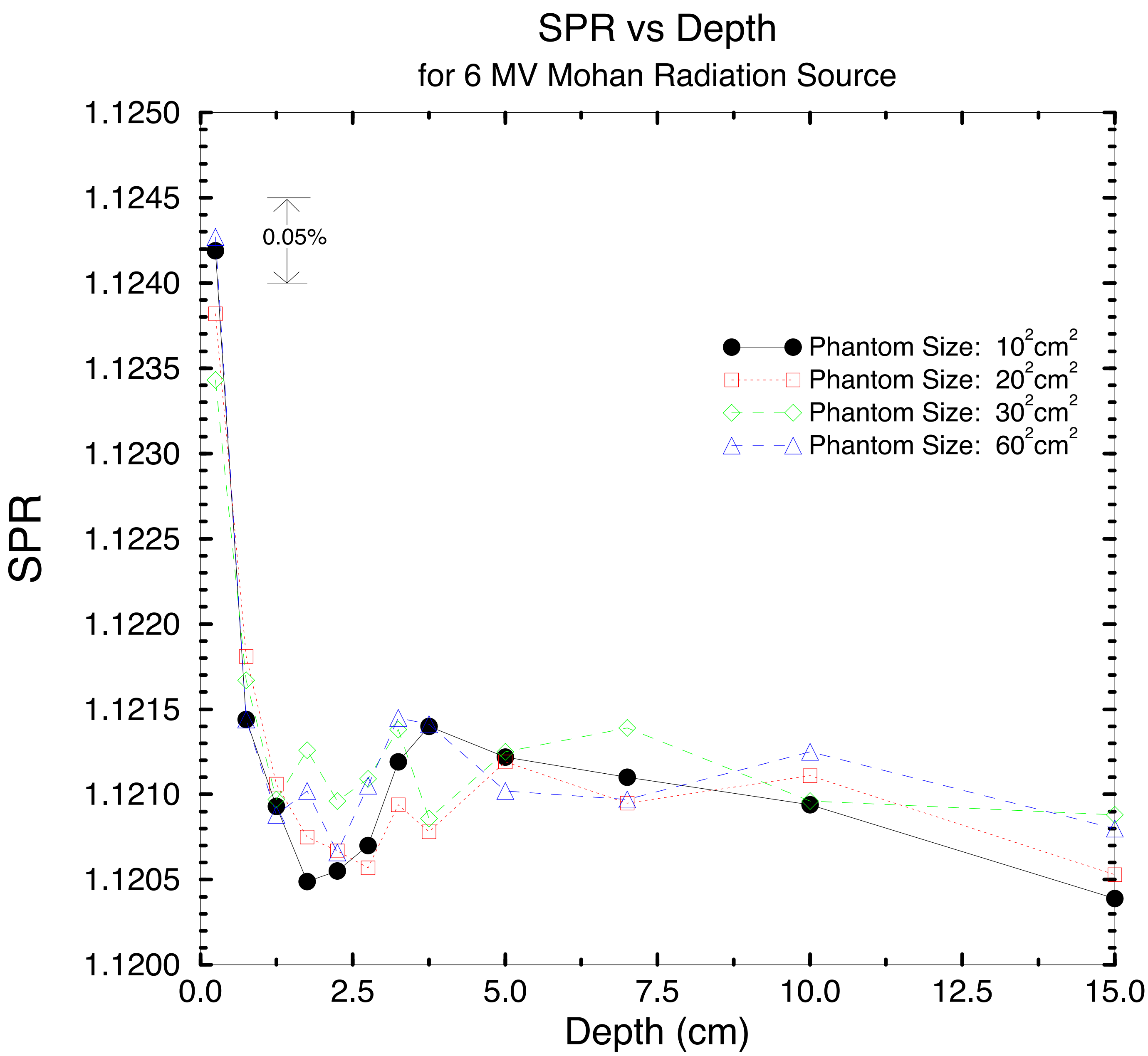

Figure 35: SPR vs depth for 6 MV Mohan source

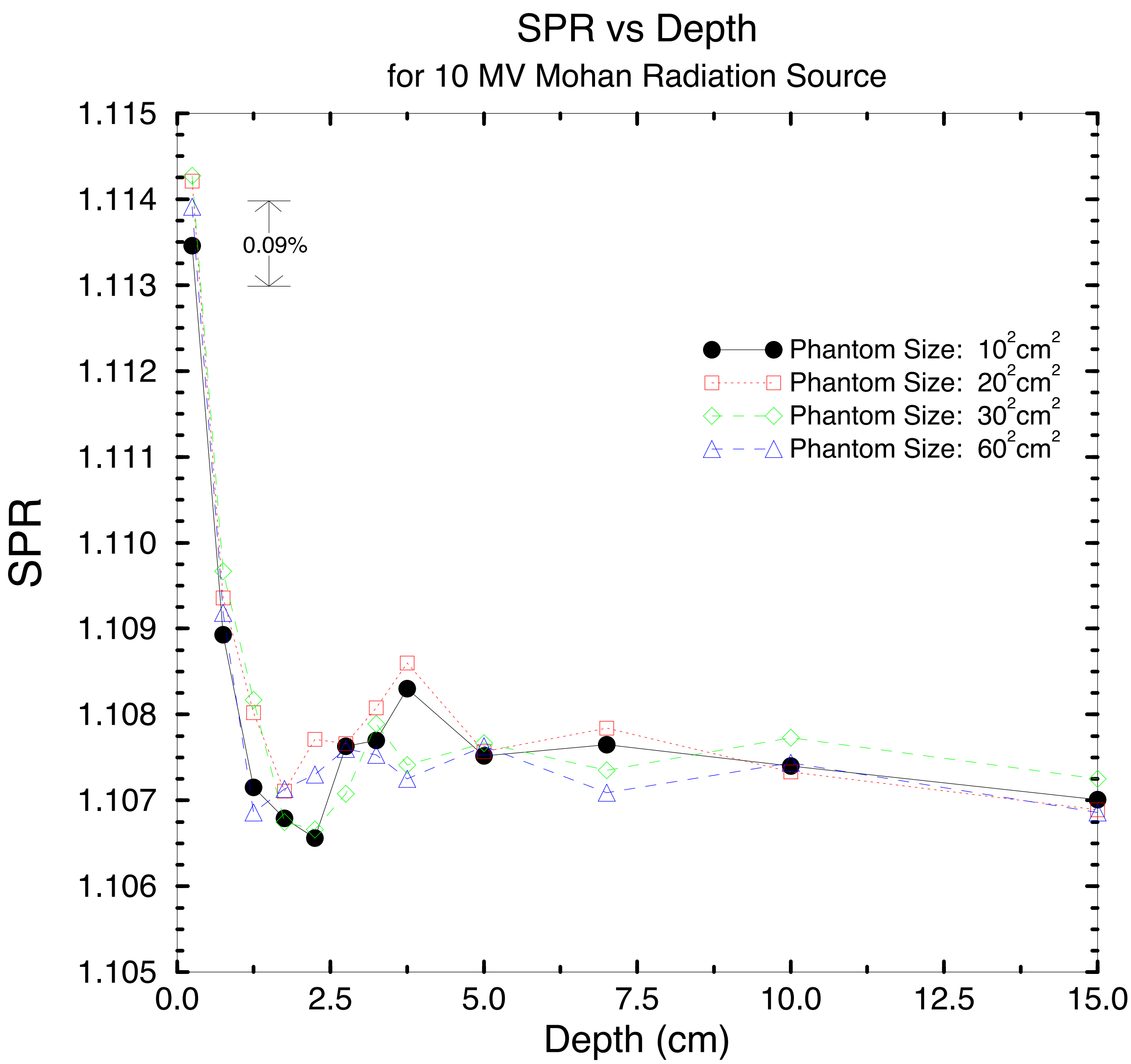

Figure 36: SPR vs depth for 10 MV Mohan source

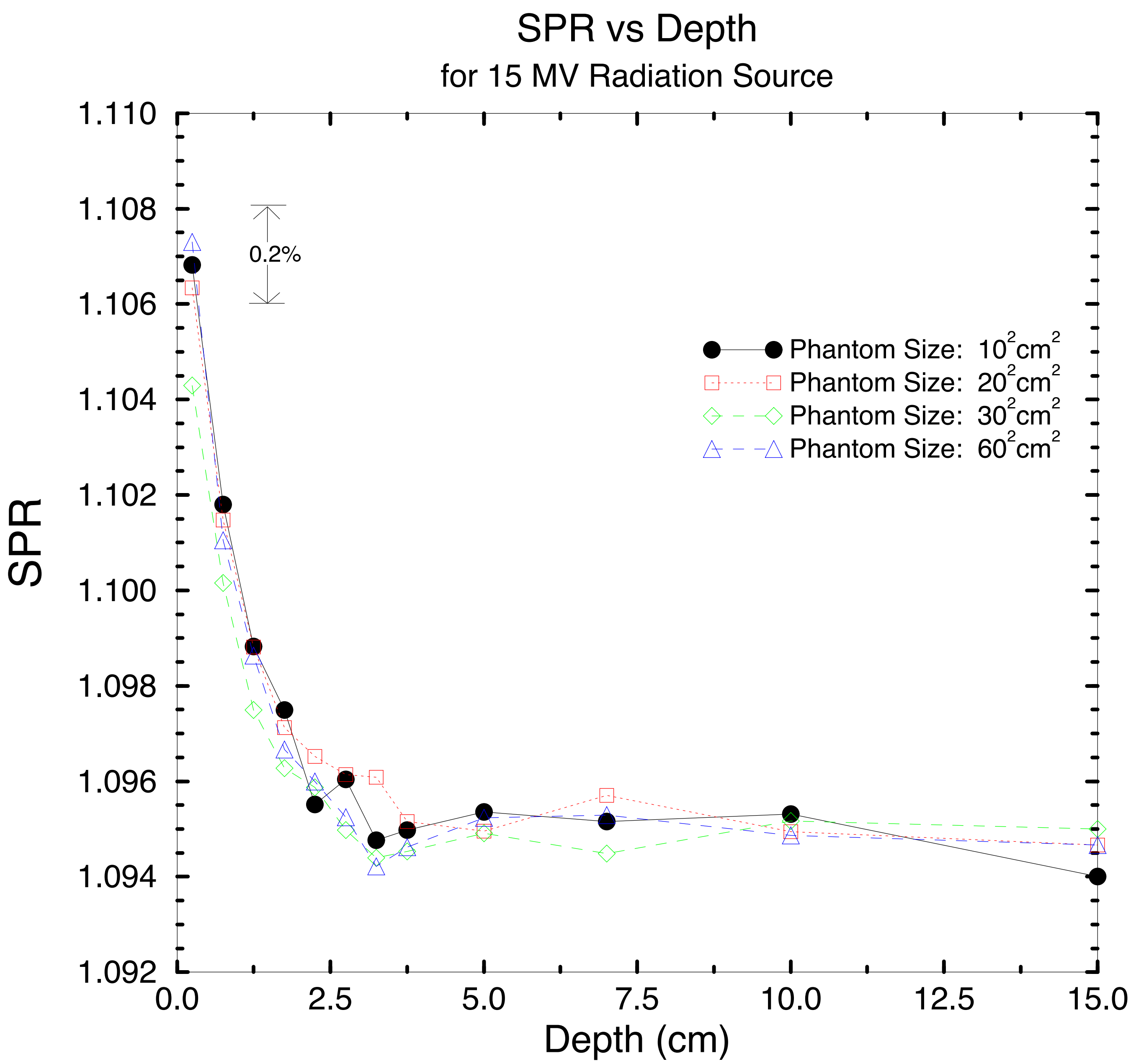

Figure 37: SPR vs depth for 15 MV Mohan source

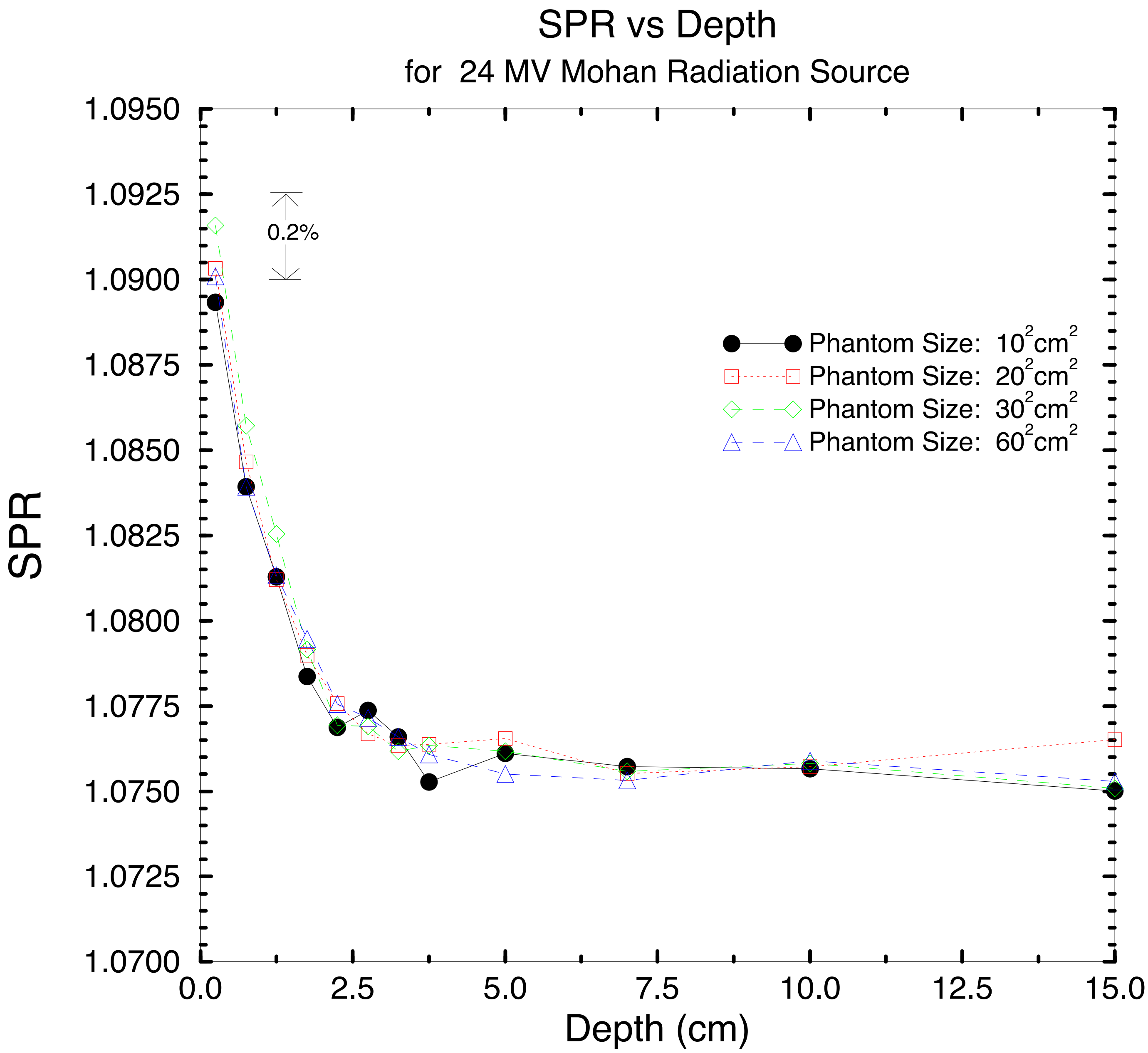

Figure 38: SPR vs depth for 24 MV Mohan source

5 Dose vs Phantom Radius

The following graphs show how the dose varies with the overall size of the phantom at depths of 5 cm, 7 cm, 10 cm, and 15 cm for different radiation point sources 100 cm from the phantom front. The beam area is 100 cm^2 in all cases. The dose data used for these graphs is from the inner most scoring region (1 cm radius) at each of the specified depths. The data has been normalized to the first data point in each series to emphasize the variation in the dose for each depth examined. The error bars indicate the uncertainty in the calculation. Typically the uncertainty is 0.1% or 0.2%.

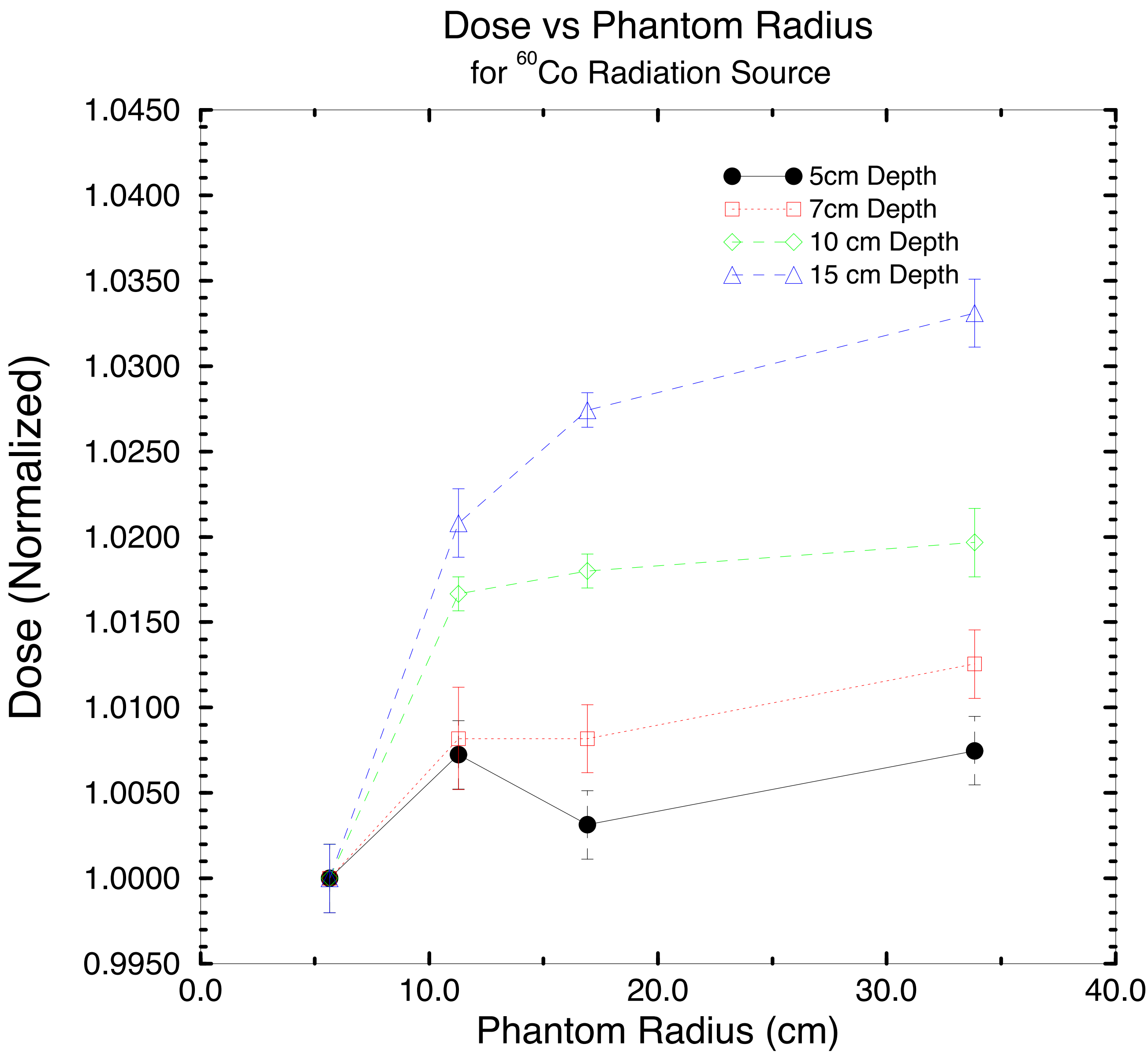

Figure 39: Dose vs phantom radius for ^{60}Co source

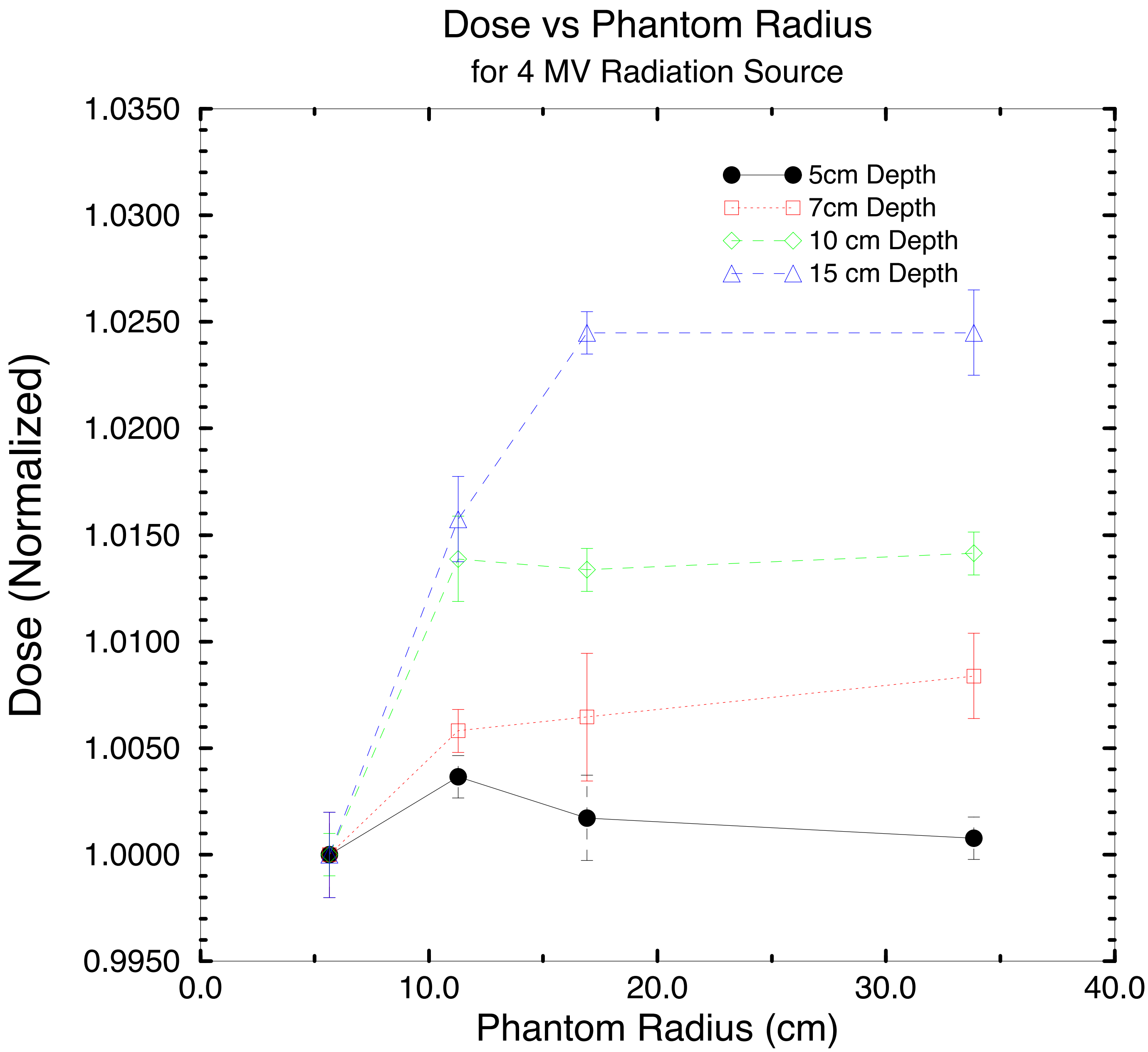

Figure 40: Dose vs phantom radius for 4 MV Mohan source

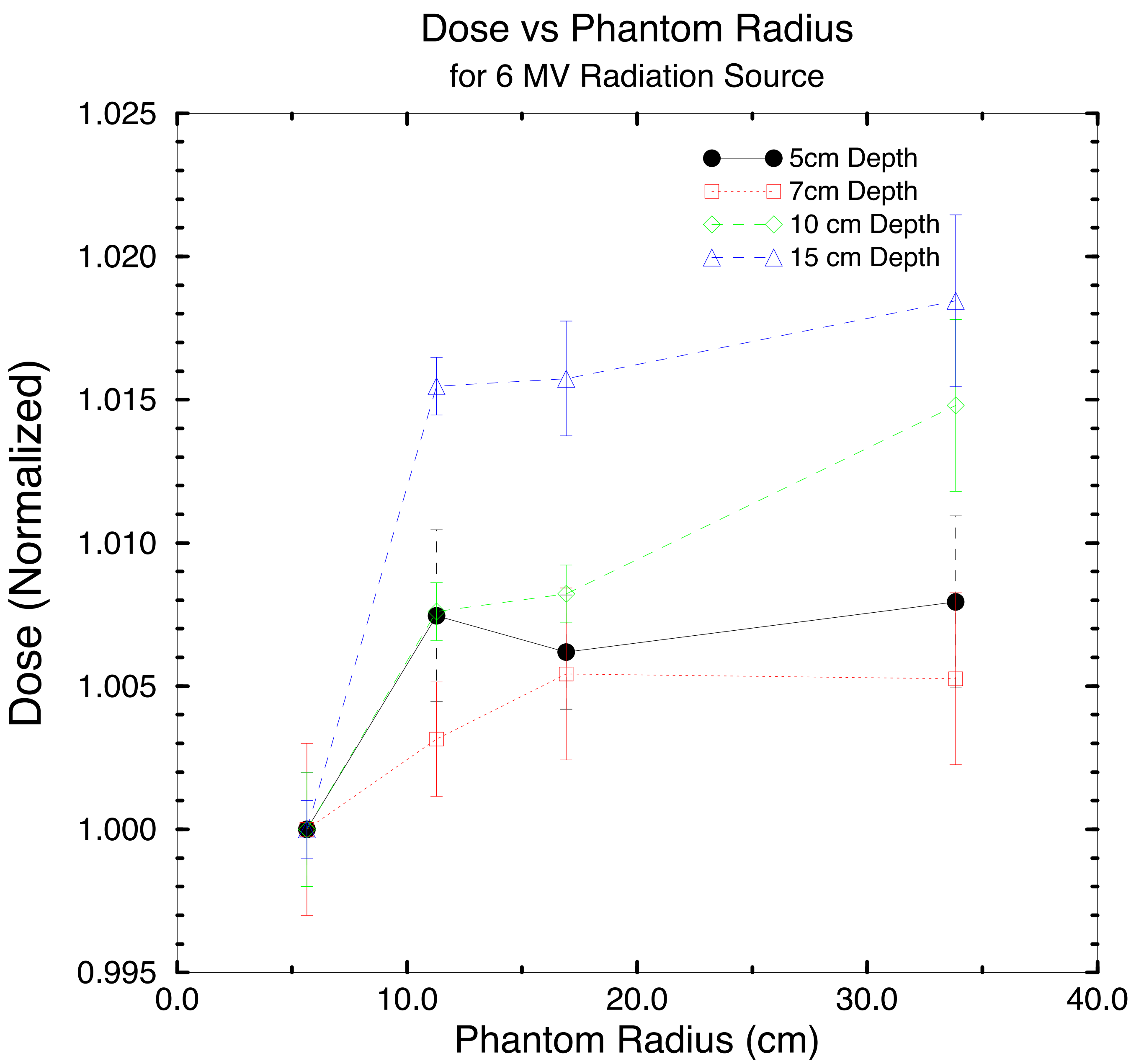

Figure 41: Dose vs phantom radius for 6 MV Mohan source

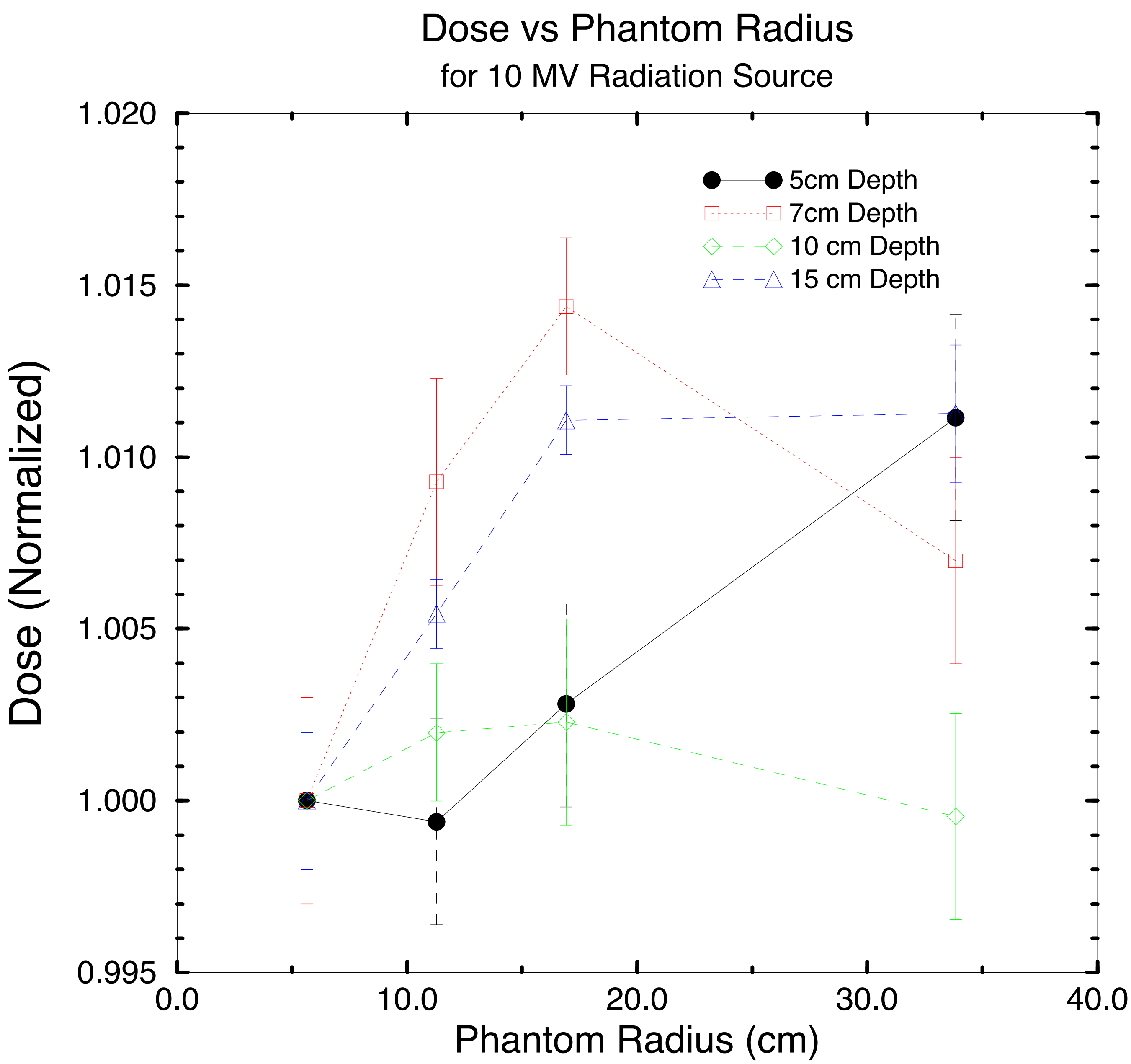

Figure 42: Dose vs phantom radius for 10 MV Mohan source

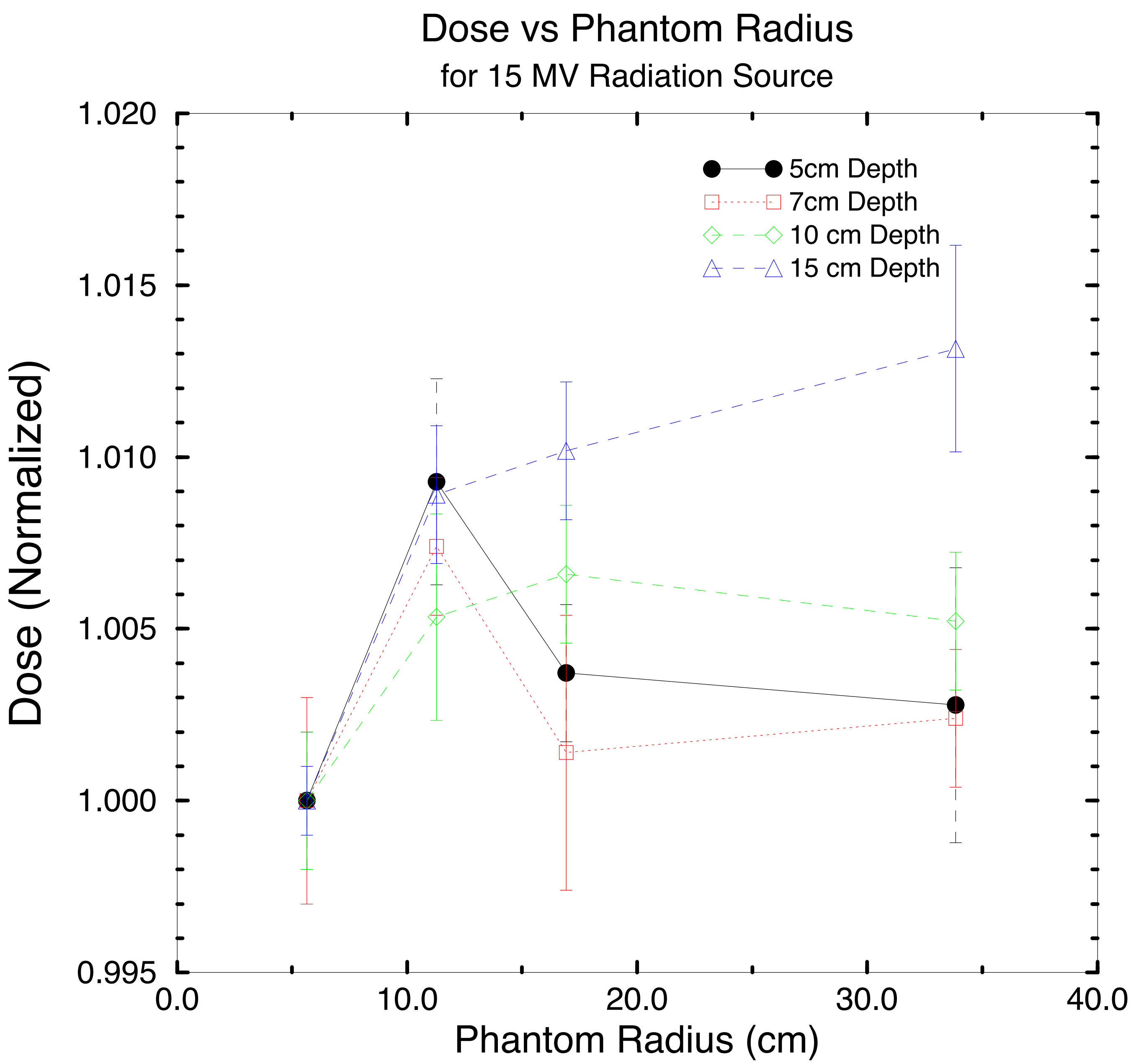

Figure 43: Dose vs phantom radius for 15 MV Mohan source

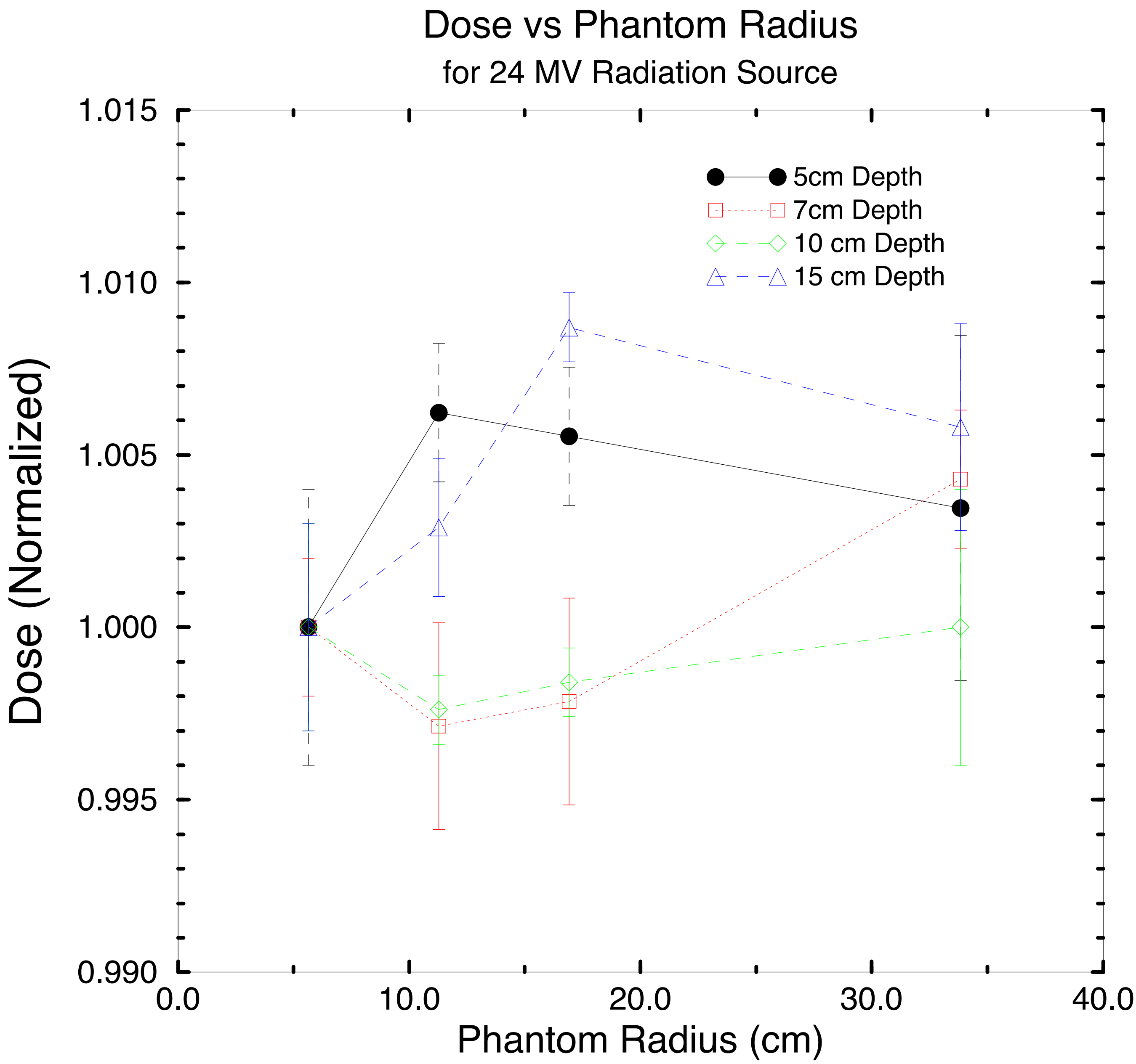

Figure 44: Dose vs phantom radius for 24 MV Mohan source

References

[1] D.W.O. Rogers, "Fundamentals of High Energy X-ray and Electron Dosimetry Protocols," in "Advances in Radiation Oncology Physics" ed J. Purdy, Medical Physics Monograph 19 (AAPM, New York) 181 – 223 (1992).

[2] D.W.O. Rogers and A.F. Bielajew, "Monte Carlo techniques of electron and photon transport for radiation dosimetry," in "The Dosimetry of Ionizing Radiation",Vol III, eds. K.R. Kase, B.E. Bjarngard, and F.H. Attix, (Academic Press) 427 – 539 (1990).

[3] A. Kosunen and D.W.O. Rogers, "DDSPR: A Code for calculating photon beam depth-dose curves and stopping-power ratios for an arbitrary spectrum," National Research Council Canada Report PIRS-298 (1992).

[4] A. Kosunen and D.W.O. Rogers, "Beam Quality Specification for Photon Beam Dosimetry," Med. Phys. **20** 1181 – 1188 (1993).

[5] G.X. Ding, D.W.O. Rogers and T.R. Mackie, "Calculation of stopping-power ratios using realistic clinical electron beams," Med. Phys. **22** 489 – 501 (1995).

[6] ICRU, "Stopping powers for electrons and positrons," Report 37, Bethesda MD (1984).

[7] S. Duane, A.F. Bielajew and D.W.O. Rogers, "Use of ICRU-37/NBS collision stopping powers in the EGS4 system," NRCC Report PIRS-0173, Ottawa, March (1989).

[8] D.W.O. Rogers, G.M Ewart, A.F. Bielajew and G. van Dyk, "Calculation of Electron Contamination in a ^{60}Co Therapy Beam," In "Proceedings of the IAEA International Symposium on Dosimetry in Radiotherapy" (IAEA, Vienna), Vol 1 303 – 312 (1988).

[9] R. Mohan, C. Chui and L Lidofsky, "Energy and angular distributions of photons from medical linear accelerators," Med. Phys. **12** 592 – 597 (1985).

[10] D.W.O. Rogers, B.A. Faddegon, G.X. Ding, C.-M. Ma, J. Wei and T.R. Mackie, "BEAM: A Monte Carlo code to simulate radiotherapy treatment units," Med. Phys. **22** (5) 503 – 524 (1995).

This was printed/latexed on July 11, 2005.